Structural optimization of polypod-like structured DNA based on structural analysis and interaction with cells

（構造解析および細胞との相互作用解析に基づく多足型 DNA 構造体の構造最適化に関する研究）

2019

Tan Mengmeng

Contents

Preface

In recent years, nucleic acid medicine is considered as a next generation medicine because of its high specificity and compatibility in organisms [1-3]. Therefore, it has been expected to be applied and treated for various diseases, such as cancer [4], pulmonary diseases [5], gene-related disease [6] and so on. Up to now, there are ten such products on the market all over the world, and seven of them were approved within the last five years, and larger numbers of nucleic acid medicine are in the preclinical phase [7] enough to their potential in the future.

Nucleic acid nanotechnology is a kind of technology that use DNA, RNA or other auxiliary materials as ingredient, so that it can produce and assembly into a two- or three-dimension structure in such a nanometer scale. DNA nanotechnology, which regards DNA as a kind of biological material, has attracted extensive attention worldwide. A typical structural property of DNA, which seems to be suitable for biomedical applications, is that it is composed of only four kinds of nucleotides, which form a double helical structure. A variety of novel materials or devices with either two- or three-dimensional DNA nanostructure have profound potential significance in biopharmaceuticals [8-11]. Um *et al*. used DNA barcodes to detect pathogenic organisms and other impurities [12]. Schmidt *et al.* designed a covalently closed (dumbbell shape) DNA molecule that possesses a stem loop structure on both sides of the double-stranded region and verified its powerful efficiency as an immunomodulatory agonist [13]. Kobiyama *et al.* developed a nanoparticle, K3-SPG, containing an immunostimulatory DNA wrapped with schizophyllan (SPG), in order to stimulate both innate and adaptive immunity [14]. Both of the potential self-assembled nanomedicines described above are in clinical tests for their practical application [15]. In addition to the aforementioned nanoparticles, self-assembled DNA nanomaterials called "DNA bricks" [16-18]. or "DNA origami" [19-21] that are constructed using a scaffold DNA and various staple strands have been invented in order to precisely design more comprehensive DNA nanostructures. In an early period, DNA origami is a representative two-dimensional conformation by precisely designing complementary pairs of sequences so that it can fold into any interesting shape [22]. Then it is developed into a three-dimensional structure gradually for clinical diagnosis [21] and drug delivery as a carrier [11]. In addition, among the three-dimensional structure designed by nanotechnology, the tetrahedron structure which shows the capacity of carrying the functional nucleic acid, such as cytosine-phosphate-guanine (CpG) DNA [23, 24] or siRNA [25], has been studied as an efficient nanostructure in the field of drug delivery system.

Branched DNA nanostructures, including Y-shaped and X-shaped DNA, have become increasingly popular in the fields of diagnostics, protein production, and drug delivery [26-28]. My laboratory has demonstrated that DNA dendrimers serve as useful carriers as well as enhancers of

immunostimulatory oligodeoxynucleotides (ODNs) that contain unmethylated CpG dinucleotides, the ligand for Toll-like receptor 9 (TLR9) [29]. In addition, previous studies from my research group has indicated that a three-dimensional nanosized polypod-like structured DNA, or polypodna, composed of three or more kinds of ODNs containing CpG motif, such as three (tripodna), four (tetrapodna), five (pentapodna), six (hexapodna), or eight pods (octapodna), could be successfully constructed by applying DNA nanotechnology that anneal the corresponding numbers of equivalent ODNs [30]. My research group also found that the polypodna structure could enhance the cell uptake efficiency of immunostimulatory DNA from immune cells such as dendritic cells and macrophages compared with traditional double- or single-strand DNA [30, 31]. Moreover, my laboratory could utilize the preferential uptake of branched DNA and incorporate immunostimulatory CpG DNA into the polypodnas, which, in turn, stimulated cytokine production in TLR9-positive cells. Based on the features which the three-dimensional polypodnas have, variety of DNA self-assembly hydrogel for antigen delivery [32] though encapsulating a tumor antigen and immune cells [33] or combining the gold nanoparticle [34] has been developed.

However, it is unclear what factors affect the structural characteristics of polypodna and how efficiently polypodna interacts with immune cells. In order to develop a polypodna suitable for disease treatment, I tried to optimize the polypodna structure based on structural analysis and interaction with cells. In Chapter 1, I focused on elucidating the orientation and bending of oligodeoxynucleotides in polypodna structure by atomic force microscopy observation. In Chapter 2, I aimed at structural analysis of polypodna with partially common sequences using small-angle X-ray scattering. In Chapter 3, I tried to demonstrate the effect of the position of CpG motif in polypodna on immune stimulation for the structural optimization.

Chapter 1　Elucidation of orientation and bending of oligodeoxynucleotides in polypod-like structured DNA by atomic force microscopy observation

（原子間力顕微鏡観察による多足型 DNA 構造体を構成する ODN 配向性の解明）

1.1 Introduction

Previous experimental results provide clear evidence that the biological activity of CpG DNA is a function of its steric structure. Since structure-dependent activity is related to cellular uptake, this relationship could be applicable to both CpG DNA and other nucleic acid-based drugs, such as antisense oligonucleotides. Therefore, it is important to understand the structural properties of these molecules to provide insight into the design of highly potent nucleic acid drugs.

Several literature reports have described the structural properties of DNA Holliday junctions and other small DNA assemblies, which were studied with various biophysical techniques, including nuclear magnetic resonance (NMR) and X-ray crystallography [35-37]. However, these methods cannot be applied to polypodnas consisting of several hundreds of nucleotides, because their size exceeds the scope of the techniques. Therefore, no detailed information is available on the structural properties of polypodnas or DNA assemblies larger than DNA Holliday junctions.

Atomic force microscopy (AFM) is a powerful tool for imaging nanosized DNA structures with high resolution. AFM has been used to characterize a variety of DNA nanostructures, such as DNA origami and DNA dendrimers [22, 38-40]. In contrast to electron microscopy, AFM can be used to investigate the structures of samples in aqueous solution. AFM images of polypodnas in a buffer solution clearly showed that all of the polypodnas (i.e., the tri-, tetra-, penta-, hexa-, and octapodna) were polypod-like structures with exactly the same number of pods as ODNs [30]. Considering that connecting polypodnas to one another results in the formation of DNA-based hydrogels [41], polypodna should be three-dimensional rather than flat or planar. In addition, the electrical repulsion and steric hindrance of the double-stranded DNA fragments of the polypodnas would also allow for the formation of a 3D structure, especially when the polypodna has four or more pods. This 3D structure, however, will be distorted under AFM imaging, since the imaging process requires the adsorption of DNA samples onto a planar mica plate. It is not clear precisely how the ODNs comprising the polypodnas are distorted under AFM imaging. Any rules concerning DNA orientation could be further used to understand the structure of complicated 3D DNA. Knowledge of these complex DNA structures might be useful for designing DNA nanostructures.

In this study, I investigated the orientation of the ODNs in a pentapodna by AFM imaging once adsorbed onto a mica plate. A DNA frame was prepared using the DNA origami method [42, 43] to visualize the flattened pentapodna in a fixed orientation. Then, I examined the AFM images of tetra- and hexapodnas for comparison with the pentapodna results.

1.2 Method and Material

1.2.1 ODNs

All ODNs used were purchased from Integrated DNA Technologies, Inc. (Coralville, IA, USA). The sequences of the ODNs are listed in Table 1. Each ODN was named as follows: the name of the polypodna, for example, pentapodna#1-4, and the number in parentheses representing the ODN number. The # and * followed by the name of polypodna were used to distinguish polypodnas having identical number of pods (4 or 5) but different sequences at the center of each ODN.

1.2.2 Preparation of polypodna

Each polypodna was prepared by mixing equimolar quantities of ODNs as previously described [16].

1.2.3 Preparation of the DNA frame and immobilization of polypodnas on the frame

The DNA frame was prepared as previously described [42, 43]. Briefly, the DNA frame was assembled in a 20 μL volume comprising final concentrations of 10 nM M13mp18 single-stranded DNA (New England Biolabs, Tokyo, Japan), 50 nM staple strands (226 strands), 20 mM Tris buffer (pH 7.6), 1 mM ethylenediaminetetraacetic acid (EDTA), and 10 mM MgCl2. The mixture was annealed by heating to 85°C and then cooling to 15°C at a rate of -1.0 °C·min^{-1}. Immobilization of the polypodnas on the frame was achieved in a solution containing the DNA frame and each polypodna (5 equivalents to the frame), by heating to 40°C and then cooling to 15°C at a rate of -1.0 °C·min^{-1} using a thermal cycler. After assembly, the sample was purified by gel-filtration (Sephacryl-400, GE Healthcare Life Sciences) to remove excess polypodna.

1.2.4 AFM imaging of polypodnas

AFM images were obtained using a high-speed AFM system (Nano Live Vision; RIBM, Tsukuba, Japan) and a silicon nitride cantilever (Olympus BL-AC10EGS) as previously reported [30, 35]. Briefly, the samples (2 μL) were adsorbed onto a freshly cleaved mica plate pretreated with 0.1% aqueous 3-aminopropyltriethoxysilane for 5 min at room temperature and then washed three times with a buffer solution containing 20 mM Tris and 10 mM $MgCl_2$. Scanning was performed in the same buffer solution.

1.2.5 Polyacrylamide gel electrophoresis

Each sample of tetra-, penta-, and hexapodna preparations was run on a 6% polyacrylamide gel at 200 V for 35 min at 4°C.

1.2.6 Melting temperature determination

The ultraviolet-melting curves of the polypodnas were obtained using a Shimadzu UV-1600 spectrophotometer (Shimadzu, Kyoto, Japan) equipped with a TMSPC-8 temperature controller. DNA samples in Tris-EDTA (TE) buffer containing 10 mM $MgCl_2$ were gradually heated from 0 to 95°C at a constant rate of 1 °C·min^{-1}. The thermal melting curves obtained were analyzed using the conventional two-point average method to obtain the melting temperature (Tm).

1.2.7 Dynamic light scattering analysis

The apparent size of polypodna was determined by the dynamic light scattering (DLS) method using a Malvern Zetasizer 3000HS (Malvern Instruments, Malvern, UK) at 20°C. The measurement was repeated at least ten times, and the results are expressed as the mean ± standard deviation of mean (SD).

Table 1. The sequences of ODNs used for polypodna preparations.

Name	Sequences (5′ → 3′)	Length (mer)
Pentapodna#1-4(01)	ATAAGAATAAACACCG TCGCTGACGTAGGCTTCAGAGTGCACTGGTACGATT TCAGTGTCAGTCAGCTTGAGCCTGTGCAAG	82
Pentapodna#1-4(02)	CTTGCACAGGCTCAAGCTGACTGACACTGA GCACTGGCATGCAGGCTCTTAGAACGTCAG	60
Pentapodna#1-4(03)	CTGACGTTCTAAGAGCCTGCATGCCAGTGC GAGCACAGATTCAGCATAGGTCATGGCAATCTGCAC	66
Pentapodna#1-4(04)	CGAGCTGAAAAGGTGG GTGCAGATTGCCATGACCTATGCTGAATCTGTGCTC AGACTGTGACTGTCTGCAGCAGAACGTCAG	82
Pentapodna#1-4(05)	CTGACGTTCTGCTGCAGACAGTCACAGTCT AATCGTACCAGTGCACTCTGAAGCCTACGTCAGCGA	66
Pentapodna*1-4(01)	ATAAGAATAAACACCG TCGCTGACGTAGGCTTCAGAGTGCACTGGTACGCTA CCTGTGTCAGTCAGCTTGAGCCTGTGCAAG	82
Pentapodna*1-4(02)	CTTGCACAGGCTCAAGCTGACTGACACAGG TAACTGGCATGCAGGCTCTTAGAACGTCAG	60
Pentapodna*1-4(03)	CTGACGTTCTAAGAGCCTGCATGCCAGTTA CCACACAGATTCAGCATAGGTCATGGCAATCTGCAC	66
Pentapodna*1-4(04)	CGAGCTGAAAAGGTGG GTGCAGATTGCCATGACCTATGCTGAATCTGTGTGG TAGCTGTGACTGTCTGCAGCAGAACGTCAG	82
Pentapodna*1-4(05)	CTGACGTTCTGCTGCAGACAGTCACAGCTA TAGCGTACCAGTGCACTCTGAAGCCTACGTCAGCGA	66
Pentapodna#1-2(01)	ATAAGAATAAACACCG TCGCTGACGTAGGCTTCAGAGTGCACTGGTACGATT GAGCACAGATTCAGCATAGGTCATGGCAATCTGCAC	88
Pentapodna#1-2(02)	CGAGCTGAAAAGGTGG GTGCAGATTGCCATGACCTATGCTGAATCTGTGCTC GCACTGGCATGCAGGCTCTTAGAACGTCAG	82
Pentapodna#1-2(03)	CTGACGTTCTAAGAGCCTGCATGCCAGTGC TCAGTGTCAGTCAGCTTGAGCCTGTGCAAG	60

Pentapodna#1-2(04)	CTTGCACAGGCTCAAGCTGACTGACACTGA AGACTGTGACTGTCTGCAGCAGAACGTCAG	60
Pentapodna#1-2(05)	CTGACGTTCTGCTGCAGACAGTCACAGTCT AATCGTACCAGTGCACTCTGAAGCCTACGTCAGCGA	66
Pentapodna*1-2(01)	ATAAGAATAAACACCG TCGCTGACGTAGGCTTCAGAGTGCACTGGTACGCTA CCTCACAGATTCAGCATAGGTCATGGCAATCTGCAC	88
Pentapodna*1-2(02)	CGAGCTGAAAAGGTGG GTGCAGATTGCCATGACCTATGCTGAATCTGTGAGG TAACTGGCATGCAGGCTCTTAGAACGTCAG	82
Pentapodna*1-2(03)	CTGACGTTCTAAGAGCCTGCATGCCAGTTA CCAGTGTCAGTCAGCTTGAGCCTGTGCAAG	60
Pentapodna*1-2(04)	CTTGCACAGGCTCAAGCTGACTGACACTGG TAGCTGTGACTGTCTGCAGCAGAACGTCAG	60
Pentapodna*1-2(05)	CTGACGTTCTGCTGCAGACAGTCACAGCTA TAGCGTACCAGTGCACTCTGAAGCCTACGTCAGCGA	66
Tetapodna#1-3(01)	ATAAGAATAAACACCG TCGCTGACGTAGGCTTCAGAGTGCACTGGTACGATT TCAGTGTCAGTCAGCTTGAGCCTGTGCAAG	82
Tetapodna#1-3(02)	CTTGCACAGGCTCAAGCTGACTGACACTGA GAGCACAGATTCAGCATAGGTCATGGCAATCTGCAC	66
Tetapodna#1-3(03)	CGAGCTGAAAAGGTGG GTGCAGATTGCCATGACCTATGCTGAATCTGTGCTC AGACTGTGACTGTCTGCAGCAGAACGTCAG	82
Tetapodna#1-3(04)	CTGACGTTCTGCTGCAGACAGTCACAGTCT AATCGTACCAGTGCACTCTGAAGCCTACGTCAGCGA	66
Tetapodna*1-3(01)	ATAAGAATAAACACCG TCGCTGACGTAGGCTTCAGAGTGCACTGGTACGCTA CCTGTGTCAGTCAGCTTGAGCCTGTGCAAG	82
Tetapodna*1-3(02)	CTTGCACAGGCTCAAGCTGACTGACACAGG TAACACAGATTCAGCATAGGTCATGGCAATCTGCAC	66
Tetapodna*1-3(03)	CGAGCTGAAAAGGTGG GTGCAGATTGCCATGACCTATGCTGAATCTGTGTTA CCACTGTGACTGTCTGCAGCAGAACGTCAG	82
Tetapodna*1-3(04)	CTGACGTTCTGCTGCAGACAGTCACAGTGG TAGCGTACCAGTGCACTCTGAAGCCTACGTCAGCGA	66
Tetapodna#1-2(01)	ATAAGAATAAACACCG TCGCTGACGTAGGCTTCAGAGTGCACTGGTACGATT GAGCACAGATTCAGCATAGGTCATGGCAATCTGCAC	88
Tetapodna#1-2(02)	CGAGCTGAAAAGGTGG GTGCAGATTGCCATGACCTATGCTGAATCTGTGCTC GCACTGGCATGCAGGCTCTTAGAACGTCAG	82
Tetapodna#1-2(03)	CTGACGTTCTAAGAGCCTGCATGCCAGTGC AGACTGTGACTGTCTGCAGCAGAACGTCAG	60
Tetapodna#1-2(04)	CTGACGTTCTGCTGCAGACAGTCACAGTCT AATCGTACCAGTGCACTCTGAAGCCTACGTCAGCGA	66
Tetapodna*1-2(01)	ATAAGAATAAACACCG TCGCTGACGTAGGCTTCAGAGTGCACTGGTACGCTA CCTCACAGATTCAGCATAGGTCATGGCAATCTGCAC	88
Tetapodna*1-2(02)	CGAGCTGAAAAGGTGG GTGCAGATTGCCATGACCTATGCTGAATCTGTGAGG TAACTGGCATGCAGGCTCTTAGAACGTCAG	82
Tetapodna*1-2(03)	CTGACGTTCTAAGAGCCTGCATGCCAGTTA CCACTGTGACTGTCTGCAGCAGAACGTCAG	60
Tetapodna*1-2(04)	CTGACGTTCTGCTGCAGACAGTCACAGTGG TAGCGTACCAGTGCACTCTGAAGCCTACGTCAGCGA	66
Hexapodna#1-2-5(01)	ACCAGTCAGGACGTTG TCGCTGACGTAGGCTTCAGAGTGCACTGGTACGATT TCAGTGTCAGTCAGCTTGAGCCTGTGCAAGATCAGT	88

Hexapodna#1-2-5(02)	ATAAGAATAAACACCG ACTGATCTTGCACAGGCTCAAGCTGACTGACACTGA CCACTGGCATGCAGGCTCTTAGAACGTCAG	82
Hexapodna#1-2-5(03)	CTGACGTTCTAAGAGCCTGCATGCCAGTGG CTGTAGTCAACGTGAGACAGCGTCTAGCAA	60
Hexapodna#1-2-5(04)	TTGCTAGACGCTGTCTCACGTTGACTACAG GAGCACAGATTCAGCATAGGTCATGGCAATCTGCAC	66
Hexapodna#1-2-5(05)	CGAGCTGAAAAGGTGG GTGCAGATTGCCATGACCTATGCTGAATCTGTGCTC AGACTGTGACTGTCTGCAGCAGAACGTCAG	82
Hexapodna#1-2-5(06)	CTGACGTTCTGCTGCAGACAGTCACAGTCT AATCGTACCAGTGCACTCTGAAGCCTACGTCAGCGA	66
Hexapodna#1-2-4(01)	ACCAGTCAGGACGTTG TCGCTGACGTAGGCTTCAGAGTGCACTGGTACGATG TCAGTGTCAGTCAGCTTGAGCCTGTGCAAGATCAGT	88
Hexapodna#1-2-4(02)	ATAAGAATAAACACCG ACTGATCTTGCACAGGCTCAAGCTGACTGACACTGA GCACTGGCATGCAGGCTCTTAGAACGTCAG	82
Hexapodna#1-2-4(03)	CTGACGTTCTAAGAGCCTGCATGCCAGTGC GAGCACAGATTCAGCATAGGTCATGGCAATCTGCAC	66
Hexapodna#1-2-4(04)	CGAGCTGAAAAGGTGG GTGCAGATTGCCATGACCTATGCTGAATCTGTGCTC AGACTGTGACTGTCTGCAGCAGAACGTCAG	82
Hexapodna#1-2-4(05)	CTGACGTTCTGCTGCAGACAGTCACAGTCT CTGTAGTCAACGTGAGACAGCGTCTAGCAA	60
Hexapodna#1-2-4(06)	TTGCTAGACGCTGTCTCACGTTGACTACAG CATCGTACCAGTGCACTCTGAAGCCTACGTCAGCGA	66
Hexapodna#1-2-6(01)	ATAAGAATAAACACCG TCGCTGACGTAGGCTTCAGAGTGCACTGGTACGATT GAGCACAGATTCAGCATAGGTCATGGCAATCTGCAC	88
Hexapodna#1-2-6(02)	CGAGCTGAAAAGGTGG GTGCAGATTGCCATGACCTATGCTGAATCTGTGCTC CCACTGGCATGCAGGCTCTTAGAACGTCAG	82
Hexapodna#1-2-6(03)	CTGACGTTCTAAGAGCCTGCATGCCAGTGG CTGTAGTCAACGTGAGACAGCGTCTAGCAA	60
Hexapodna#1-2-6(04)	TTGCTAGACGCTGTCTCACGTTGACTACAG TCAGTGTCAGTCAGCTTGAGCCTGTGCAAG	60
Hexapodna#1-2-6(05)	CTTGCACAGGCTCAAGCTGACTGACACTGA AGACTGTGACTGTCTGCAGCAGAACGTCAGCTGCAC	66
Hexapodna#1-2-6(06)	ACCAGTCAGGACGTTG GTGCAGCTGACGTTCTGCTGCAGACAGTCACAGTCT AATCGTACCAGTGCACTCTGAAGCCTACGTCAGCGA	88

and * are used to distinguish polypodna having different sequences at the center of each ODN.

1.3 Results and Discussion

1.3.1 ODN orientation in DNA frame

The ODNs that comprise the pentapodna must be bent near the center to form the pentapod-like structure. Then, the ODNs can be in either of the following two conformations: (1) The ODNs are slightly bent and cross one another at the center of the pentapodna, where the bending angle of each ODN should be 144° under the assumption that all the pod parts are equivalent (Figure 1), the cross-type conformation); or (2) the ODNs sharply bend at an angle of 72° at the center (the bend-type

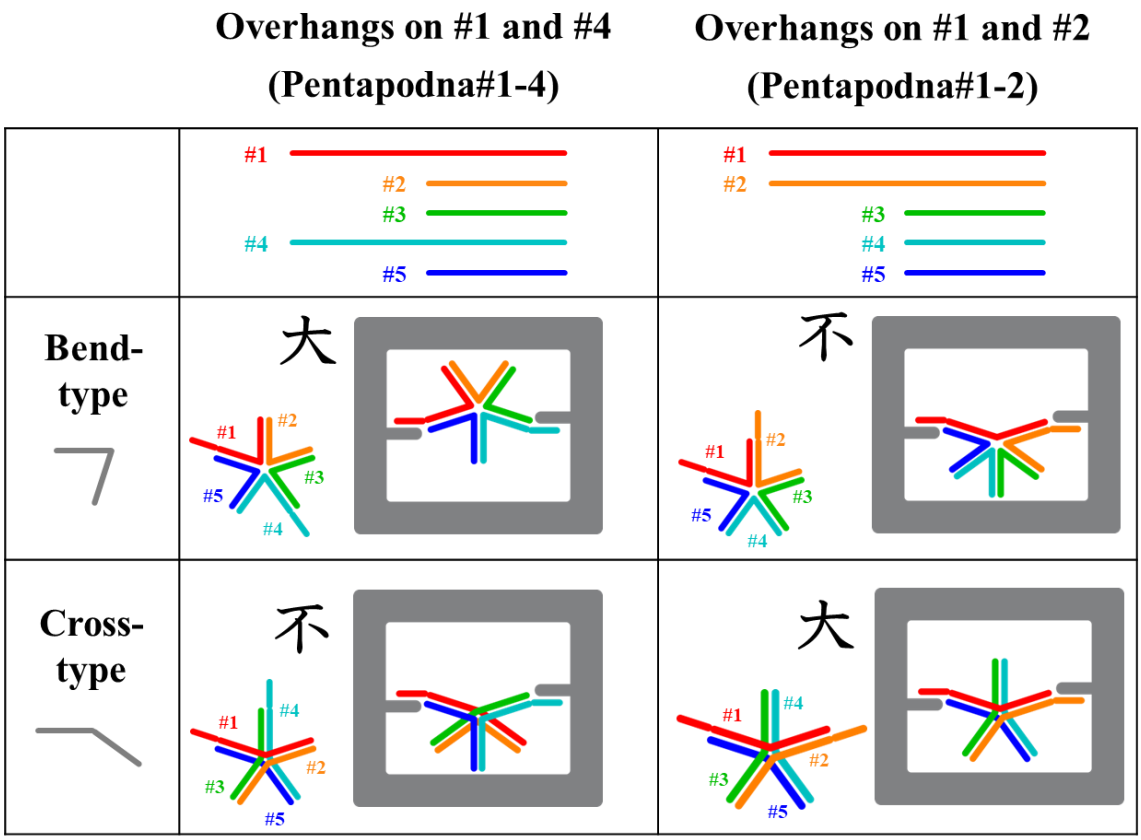

Figure 1. Estimated planer images of ODN orientation in DNA frame. The estimated planar images of pentapodna#1-4 and pentapodna#1-2 were drawn with the assumption that the ODNs are in the bend-type conformation (top) or in the cross-type conformation (bottom). Each ODN is marked with a different color: ODN#1, red; ODN#2, orange; ODN#3, green; ODN#4, cyan; and ODN#5, blue. The grey rectangles are the DNA origami frames.

conformation). To determine which conformation would be preferred, I designed two pentapodnas that had two long single-stranded sequences on the 5'-end of the two ODNs that were immobilized on the DNA frame. The long sequences in pentapodna(1-4) were located on ODNs #1 and #4, and on ODNs #1 and #2 in pentapodna(1-2). If the ODNs were in the cross-type conformation, pentapodna(1-4) would present all three free pods to one side of the connecting ODNs, whereas pentapodna(1-2) would present one free pod on one side and the other two pods on the other side. The converse results would be obtained if the ODNs were in the bend-type conformation.

1.3.2 Physical properties of polypodna

Prior to AFM imaging, the formation of the pentapodnas, as well as tetrapodnas and hexapodnas, was confirmed by polyacrylamide gel electrophoresis (PAGE) (Figure 2). Each sample had a major single band with a mobility that corresponded to the number of its pods, indicating that all of the polypodnas were successfully formed under the described conditions. The melting temperatures

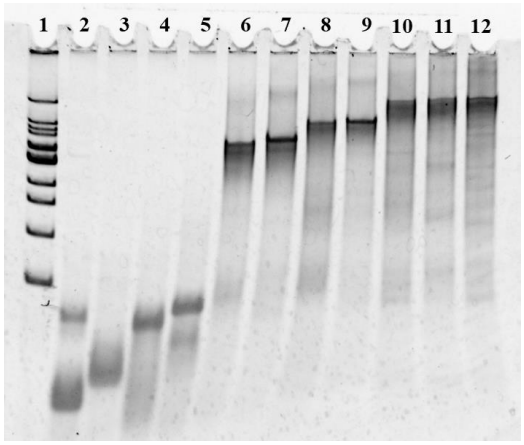

Figure 2A. Polyacrylamide gel electrophoresis (PAGE) analysis of tetra-, penta-, and hexapodna preparations. Each sample was run on a 6% polyacrylamide gel at 200 V for 20 min at 4°C. Lane 1, 100-bp DNA ladder; lane 2, ssDNA60; lane 3, ssDNA66; lane 4, ssDNA82; lane 5, ssDNA88; lane 6, tetrapodna(1-3); lane 7, tetrapodna(1-2); lane 8, pentapodna(1-4); lane 9, pentapodna(1-2); lane 10, hexapodna(1-2-5); lane 11, hexapodna(1-2-4); lane 12, hexapodna(1-2-6).

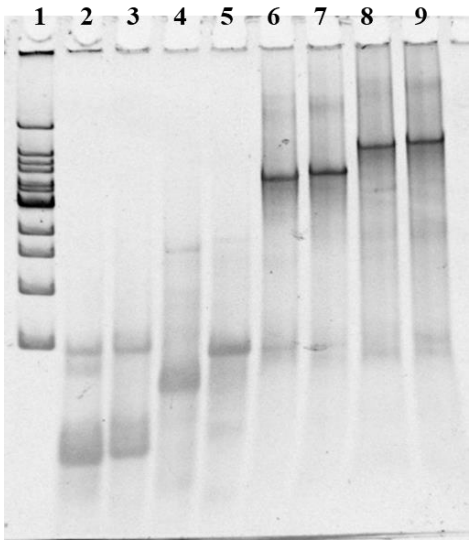

Figure 2B. Polyacrylamide gel electrophoresis (PAGE) analysis of tetra- and pentapodna preparations. Each sample was run on a 6% polyacrylamide gel at 200 V for 35 min at 4°C. Lane 1, 100-bp DNA ladder; lane 2, ssDNA60; lane 3, ssDNA66; lane 4, ssDNA82; lane 5, ssDNA88; lane 6, tetrapodna(1-3); lane 7, tetrapodna(1-2); lane 8, pentapodna(1-4); lane 9, pentapodna(1-2).

DNA	Tm (°C)	Size (nm)
Tetrapodna#1-3	78.4	10.8 ± 1.0
Tetrapodna*1-3	78.7	10.9 ± 0.9
Tetrapodna#1-2	78.6	11.8 ± 0.3
Tetrapodna*1-2	78.7	10.9 ± 1.1
Pentapodna#1-4	76.9	11.5 ± 0.4
Pentapodna*1-4	77.7	11.5 ± 0.7
Pentapodna#1-2	77.2	11.9 ± 0.7
Pentapodna*1-2	77.5	13.0 ± 0.6
Hexapodna#1-2-5	75.9	12.7 ± 1.3
Hexapodna#1-2-4	76.4	12.6 ± 1.3
Hexapodna#1-2-6	76.4	11.6 ± 0.9

Table 2. Tm and apparent size of each polypodna. The melting temperature (Tm) was calculated from the melting curves of polypodna preparations in a TE buffer solution (pH 8) containing 10 mM magnesium chloride. The apparent size was measured by DLS and expressed as the mean ± S.D. of ten determinations.

of the polypodnas were determined by measuring the temperature-dependent absorbance at 260 nm. A previous study from my laboratory revealed that Tm was inversely correlated with the pod number, when all the attached ODNs were of the same length [30]. Although the Tms of the polypodnas used in this study were nearly comparable, I did observe a reduction in Tm with increasing pod number (Table 2). Next, the apparent size was measured using DLS, assuming a noncircular polypodna shape. The preparations showed a narrow size distribution with a range from 10 to 13 nm (Table 2).

1.3.3 AFM images of pentapodna#/*1-4 and pentapodna#/*1-2

Figure 3 shows the AFM images of pentapodna#1-4 (left) and pentapodna*1-4 (right). The images revealed that the pentapodna was connected to the frame through the two long single-stranded

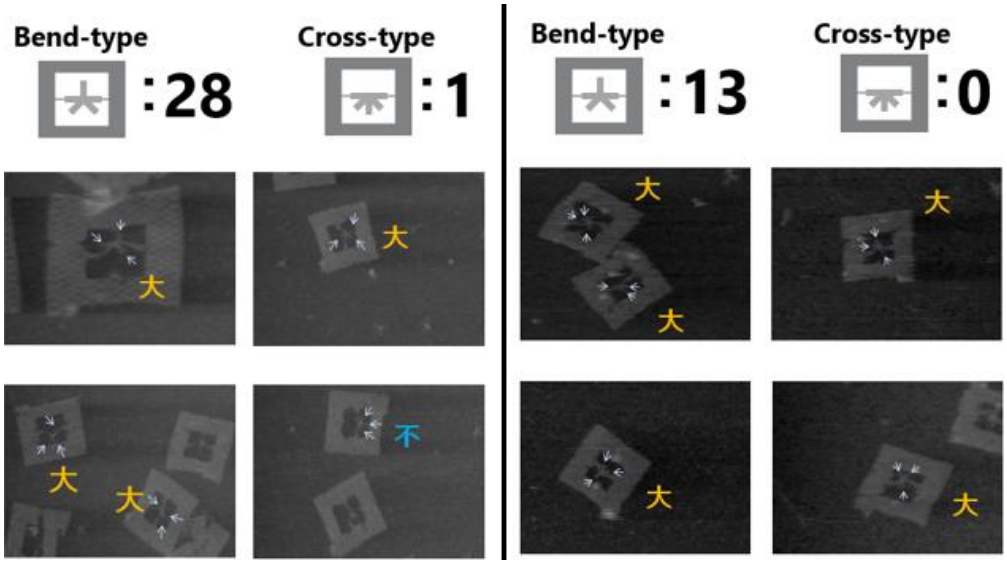

Figure 3. The AFM images of (left) pentapodna#1-4 and (right) pentapodna*1-4 are shown. Arrows indicate the free pods of the pentapodna. Image sizes: 200 nm × 150 nm (upleft images); 400 nm × 300 nm (other images). Arrows indicate the free pods of pentapodna.

sequences on ODNs #/*1 and #/*4, although some distorted structures were also observed. The yield for the incorporation of pentapodna#1-4 to the DNA frame was 69% (36 out of 52). Counting the number of pentapodna in the bend-type (the three free pods are split, with one and two pods on either side, respectively) or cross-type (all three pods are on the same side) conformation indicated that more than 90% of the pentapodnas were in the bend-type conformation (28 bend-type, 1 cross-type and 7 unidentified for pentapodna#1-4; 13 bend-type and 0 cross-type for pentapodna*1-4). These results suggest that ODNs in the pentapodnas primarily form the bend-type conformation.

Another possibility is that the three free pods cannot be localized to one side of the pentapodna because of electrical repulsion or steric hindrance. If this is the case, the AFM images do not support the idea that the ODNs of pentapodnas are in the bend-type conformation. Therefore, I also observed pentapodna#1-2 and pentapodna*1-2 using AFM (Figure 4). The yield for the incorporation of pentapodna#1-2 onto the DNA frame was 76% (34 out of 45). The AFM images showed that 23 out of the 25 pentapodna#1-2 (92%, 9 unidentified) and all (12) of the pentapodna*1-2 exhibited three free

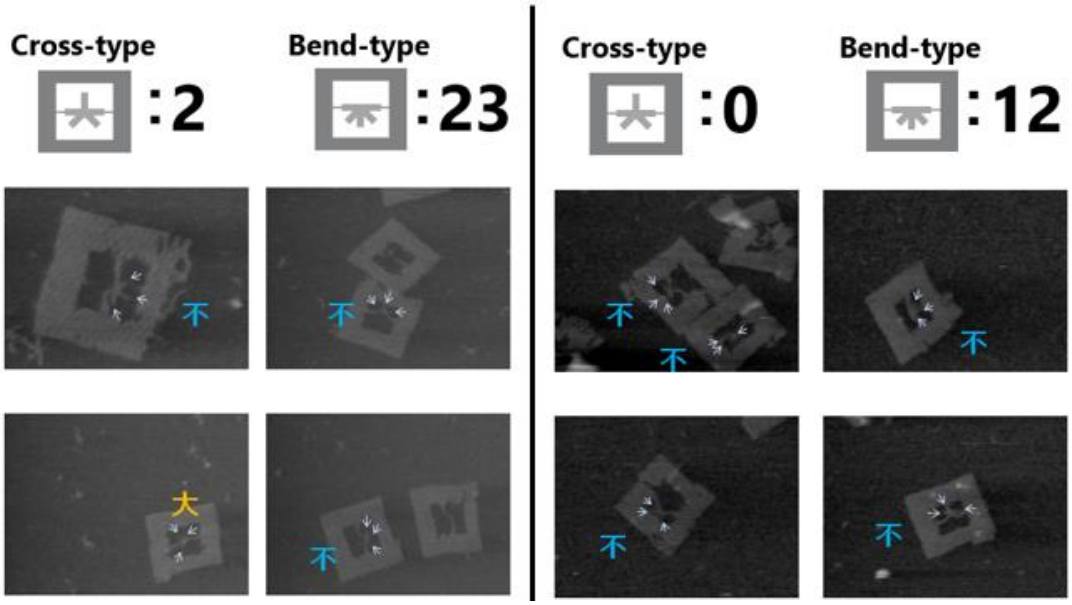

Figure 4. The AFM images of (left) pentapodna#1-2 and (right) pentapodna*1-2 are shown. Arrows indicate the free pods of the pentapodna. Image sizes: 200 nm × 150 nm (upleft images); 400 nm × 300 nm (other images). Arrows indicate the free pods of pentapodna.

pods on the same side, and were therefore in the bend-type conformation. Taken together with the results of pentapodna#/*1-4, these data strongly suggest that the ODNs of pentapodnas are in the bend-type conformation and sharply (72° on average) bend at the center.

1.3.4 AFM images of tetrapodna#/*1-3 and tetrapodna#/*1-2

To validate the results obtained using the pentapodnas, I next used two tetrapodnas: tetrapodna#/*1-3 (Figure 5 left) and tetrapodna#/*1-2 (Figure 5 right). Tetrapodna#1-3 has long sequences on ODNs #1 and #3, and tetrapodna#1-2 has long sequences on ODNs #1 and #2. Figure 5 shows the estimated planar images of these tetrapodnas in the bend-type conformation. The yields for the incorporation of tetrapodna#1-3 and tetrapodn#1-2 onto the DNA frame were 50% (23 out of 46) and 84% (42 out of 50), respectively. The AFM images showed that 13 out of the 14 tetrapodna#1-3 (93%, 9 unidentified) and all 18 tetrapodna*1-3 (100%) had a free pod on one side and another on the other side, whereas 27 out of 28 tetrapodna(1-2) (96%, 14 unidentified) and all 12 tetrapodna*1-2 (100%) presented both free pods on the same side of the connecting ODNs. These results are in

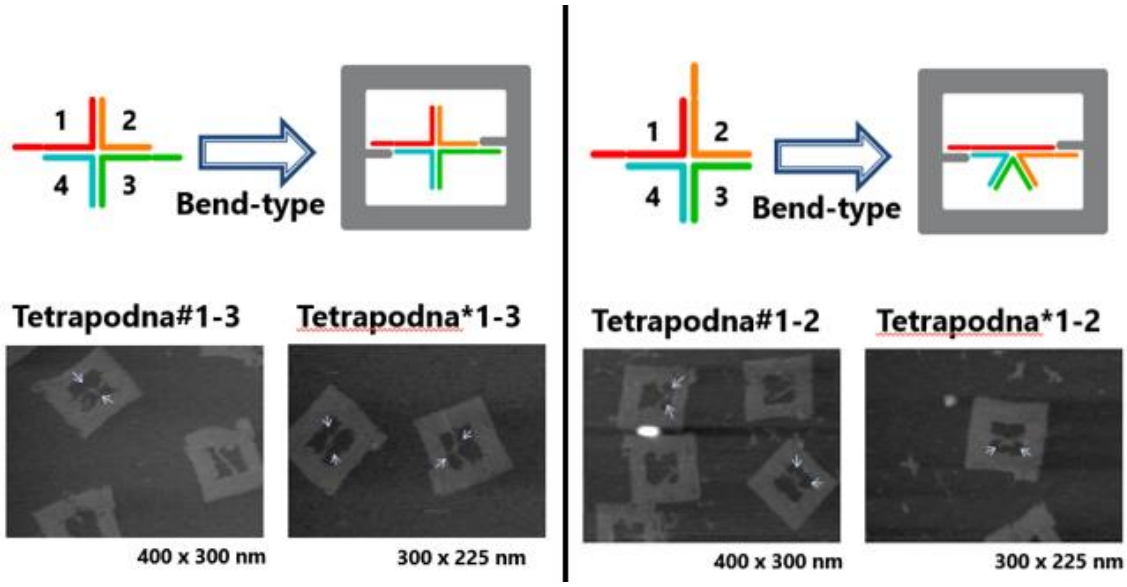

Figure 5. Estimated planar images and AFM images of tetrapodnas. The estimated planar images of tetrapodna#/*1-3 and tetrapodna#/*1-2 were drawn with the assumption that the ODNs are in the bend-type conformation. Each ODN is marked with a different color: ODN #1, red; ODN #2, orange; ODN #3, green; and ODN #4, cyan. The AFM images of tetrapodna#/*1-3 and tetrapodna#/*1-2 are shown. Arrows indicate the free pods of the tetrapodna. Image size: 400 nm × 300 nm (left); 300 nm × 225 nm (right).

agreement with the estimated planar images drawn with the assumption that the ODNs are in the bend-type conformation.

1.3.5 AFM images of hexapodna#1-2-5, #1-2-4 and #1-2-6

I next tried to determine the orientation of the ODNs in the hexapodna. I first designed hexapodnas with two long single-stranded sequences on the 5'-end of the two ODNs, similar to the penta- and tetrapodnas. However, it is worth mentioning that it was difficult to judge the orientation of the four free pods in the DNA frame. Next, I used another DNA frame, to which a hexapodna was immobilized through three pods, and designed three hexapodnas: hexapodna#1-2-5, hexapodna#1-2-4, and hexapodna#1-2-6), in which the numbers in parenthesis indicate the ODN numbers with the long, single-stranded sequences. Figure 6 shows the estimated planar images and AFM images of hexapodna#1-2-5, hexapodna#1-2-4, and hexapodna#1-2-6. Again, the images were drawn with the assumption that all of the ODNs were in the bend-type conformation. Each side of the DNA frame was named A, B, C, or D, with the former three containing the extruding ports. The yield for the incorporation of the hexapodna onto the DNA frame was much lower than those of the penta- and tetrapodna, and only 7 (hexapodna#1-2-5), 9 (hexapodna#1-2-4), and 2 (hexapodna#1-2-6) hexapodnas were observed as immobilized on the frames, even though 40 or more DNA frames were checked by AFM. For the immobilized hexapodna#1-2-5, almost all samples were configured with

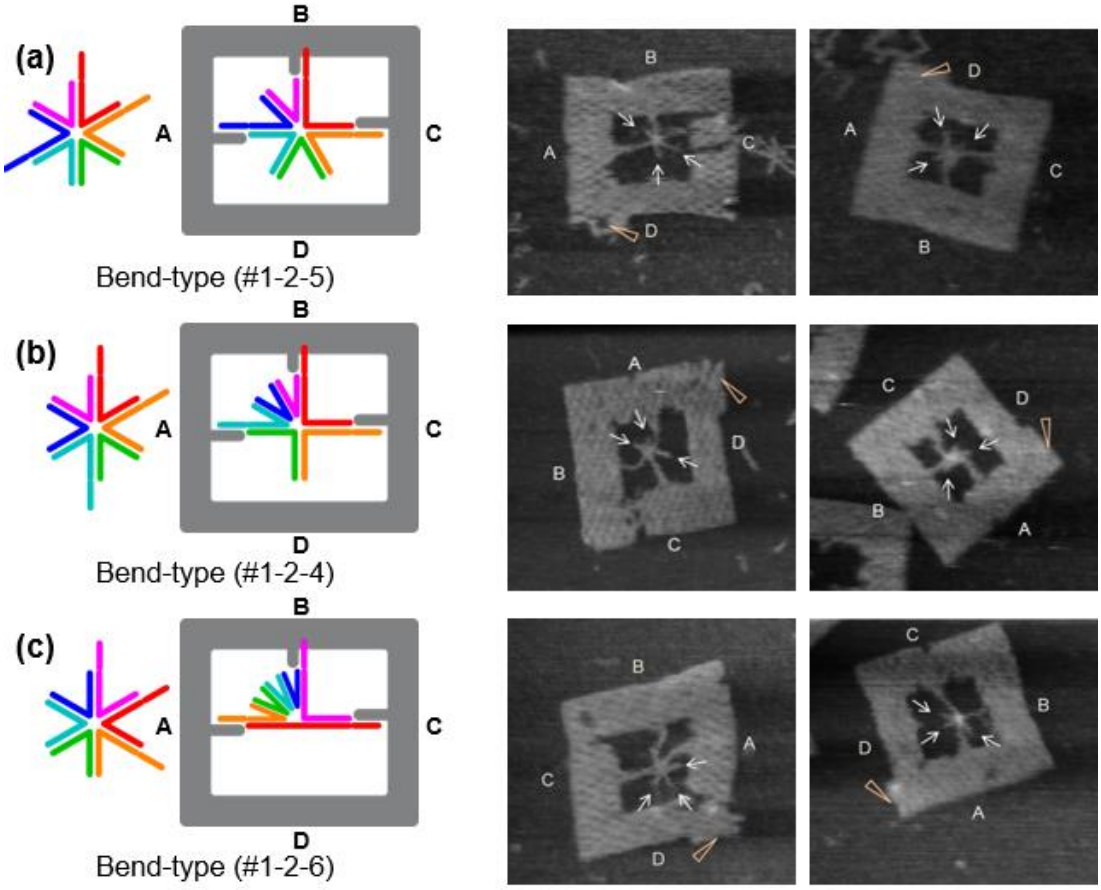

Figure 6. Estimated planar images and AFM images of hexapodnas. Estimated planar images of (a) hexapodna#1-2-5, (c) hexapodna#1-2-4, and (e) hexapodna#1-2-6 were drawn with the assumption that the ODNs are in the bend-type conformation. Each ODN is marked with a different color: ODN #1, red; ODN #2, orange; ODN #3, green; ODN #4, cyan; ODN #5, blue; and ODN #6, pink. The AFM images of (b) hexapodna#1-2-5, (d) hexapodna#1-2-4, and (f) hexapodna#1-2-6 are shown. Arrows indicate the free hexapodna pods. Arrowheads indicate the right-bottom corner of the DNA frame for orientation. Image size: 240 nm × 180 nm.

one free pod in the AB corner and the other two on side D (Figure 6(b)). This result was in concordance with the estimated planar image (Figure 6(a)). By contrast, 3 out of 9 hexapodna#1-2-4 were captured in the bend-type conformation, while the other 6 were not (Figure 6(d)). No AFM images were obtained in which hexapodna#1-2-6 had ODNs in the bend-type conformation (Figure 6(f)). If the ODNs in the hexapodna naturally take on the bend-type conformation under unconstrained conditions, hexapodna#1-2-6 should have the largest steric hindrance, since the three free pods are required to be arranged in one narrow corner, AB. This very distorted and imbalanced structure was not observed in the present study, suggesting that the steric hindrance of the pods should be considered when polypodna are adsorbed onto a mica plate. By contrast, hexapodna#1-2-5, which should exhibit the least steric hindrance among the samples prepared, was captured with the ODNs in the bend-type conformation. These considerations strongly support the hypothesis that ODNs tend to take on the

bend-type conformation under unconstrained conditions, but that this conformation is forced to change as the steric hindrance increases.

Previous studies reported that the sequences around the junction of branched DNAs, such as DNA Holliday junctions, played significant roles in their conformations [44–46]. To examine the role of the sequences on the conformations of the tetra- and pentapodna, different sets of each were designed and prepared: pentapodna*1-4, pentapodna*1-2, tetrapodna*1-3, and tetrapodna*1-2. For these DNA samples, sequences near the junction with typically reported bending angles of ~43° were employed [46]. The AFM images of each polypodna with the selected sequences were comparable to those of the polypodnas without the sequences (Figure 4 and 5), and showed again that the ODNs in these tetrapodnas are in the bend-type conformation. In addition, the zoom-out AFM images showed that these polypodnas were quite efficiently incorporated into the DNA frame (Figure 7). Then, the

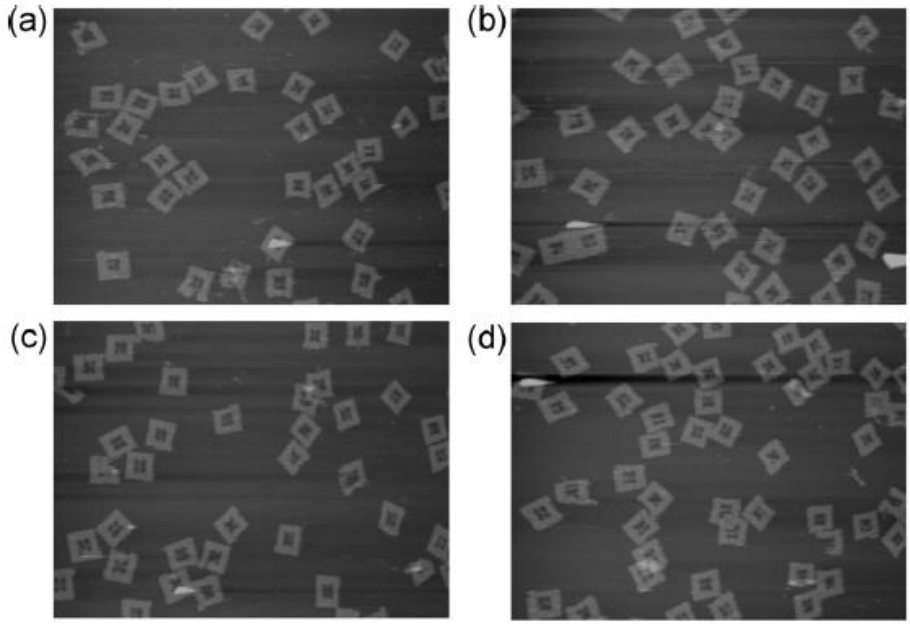

Figure 7. Zoom-out AFM images of (a) pentapodna*(1-4), (b) pentapodna*(1-2), (c) tetrapodna*(1-3), and (d) tetrapodna*(1-2). Image size: 1,200 nm × 900 nm.

AFM images of tetrapodna#1-3 and tetrapodna*1-3 were used to estimate the angle of the junction: The acute angles were $54.7^{\circ} \pm 8.8$ and $53.3^{\circ} \pm 5.1$, respectively, and there were no significant differences between them. These results suggest that the sequence around the junction has little effect on the bending angle or orientation of the ODNs, as far as the planar AFM images of polypodna are concerned.

Short double-stranded DNA is one of the stiffest natural polymers and is unlikely to bend sharply, in contrast to single-stranded DNA. The stiffness of double-stranded DNA can be a potential

obstacle for designing and preparing DNA nanostructures [47]. By contrast, it has recently been reported that double stranded DNA of 100 base pairs or less is somewhat flexible [48]. Therefore, the actual stiffness or flexibility of double-stranded DNA remains an open question. The observed trend of decreasing Tm with increasing pod number for the polypodnas indicates that the hybridization efficiency of the double-stranded portion of the polypodna is reduced with increasing pod number. These results can be explained by the following factors. First, the bases closest to the bending site hybridize less efficiently than the portions of unconstrained, straight DNA. In addition, the efficiency will decrease as the bending angle becomes more acute. If the ODNs can take up the cross-type conformation, polypodna with eight or more pods, such as octapodna (eight pods) and dodecapodna (twelve pods), may be more easily formed than hexapodna. This is because the bending angle is minimal (90°) with a pod number of only six when the polypodnas are freely floating in solution. However, a dodecapodna was not formed when twelve 36-mer ODNs were annealed [30]. These results further support the idea that the ODNs in the polypodna are in the bend-type conformation.

It is an open question whether the difference in the size between tetrapodna and a smaller DNA Holliday junction influences their structural properties. A prior X-ray crystallography study showed that a DNA Holliday junction can adopt either an open extended-X conformation or a more compact stacked-X conformation. It was also reported that the type of cation influenced the conformation of the junction [37]. Although more studies are needed, there seems to be no apparent discrepancy between the conformations of the reported DNA Holliday junctions and that proposed for the tetrapodna in the present study.

Chapter 2　Structural analysis of polypod-like structured DNA with partially common sequences using small-angle X-ray scattering

（小角 X 線散乱法による部分的共通配列を含む多足型 DNA 構造体の構造解析）

2.1 Introduction

Various methods have been adopted to resolve three-dimensional DNA nanoparticles, such as atomic force microscopy (AFM) [49, 50], wide-angle X-ray scattering [51, 52], fluorescence resonance energy transfer [53, 54], computer simulation [55, 56], and crystallization [57, 58]. In chapter 1, I elucidated the orientation and bending of ODNs in polypodnas using AFM successfully, and demonstrated that the polypodnas, i.e., the tetra-, penta-, and hexapodnas, adopt the bend-type conformation when the structures are flattened under unconstrained conditions. In addition, small-angle X-ray scattering (SAXS) is a method used to analyze DNA structures in the range of 0.1-100 nm in solution. Sanada *et al.* verified the relationship between the radius of gyration (Rg) and immunostimulatory activity of polypodna using SAXS and computer simulation methods [59, 31]. Im *et al.* demonstrated that Y-shaped and X-shaped DNAs adopted a B-form conformation in solution using SAXS analysis [60].

Oligodeoxynucleotide (ODN)-based DNA nanostructures are promising delivery vehicles for the delivery of bioactive agents, including immunostimulatory DNA, whereas the use of many kinds of ODNs may increase the possibility of off-target or unintentional effects [61, 62] and raise a safety concern in clinical applications of ODN-based DNA nanostructures in the future. One possible solution is to employ a set of ODNs with blocks of common sequences, since the desirable and undesirable biological activities of ODNs mainly depend on the sequence. In general, the parts of DNA nanostructures consist of double-stranded DNA, and this characteristic limits the sequence variation of the ODNs used for DNA nanostructures. The palindrome sequence, which is a section of DNA or RNA that possesses the same base-pairs reading from 5’ to 3’ on one strand and from 3’ to 5’ on the complementary strand [63, 64], is a suitable candidate for such common sequences. Hypothetically, polypodna can be constructed using ODNs with fully palindromic sequences. The section of palindrome sequences in ODNs, however, possesses the flexibility that may result in various intramolecular tertiary structures or conformations within DNA nanostructures. As the interaction of DNA nanostructures and cells is mainly determined by their tertiary structural features [30, 31, 59], it is necessary to figure out the structural properties of the ones consisting of ODNs with common sequences in order to optimally design DNA nanostructures.

Here, I designed several types of tetrapod-like structured DNA, or tetrapodna, each of which consists of four 36-base ODNs. A symmetrical tetrapodna, Tet(sym), was designed using four ODNs with sequences different from one another. Then, either 8, 12, or 16 bases in the central part of the four ODNs of Tet(sym) were changed to common sequences of 5’-AGCATGCT-3’, 5’-ATAGCATGCTAT-3’, or 5’-CGATAGCATGCTATCG-3’, in order to obtain tetrapodnas with blocks

of identical palindromic sequences, Tet(id8), Tet- (id12), and Tet(id16), respectively. In addition, 2 types of asymmetric tetrapodna, Tet(asym12) and Tet(asym16), were also designed, because Tet(id12) and Tet(id16) may possibly have similar structures as Tet(asym12) and Tet(asym16), respectively. The formation of these sets of tetrapodnas was evaluated, and their structural features were analyzed using SAXS. Finally, their cell interaction was investigated in order to estimate their potential and significance in biological or clinical applications.

2.2 Materials and Methods

2.2.1 Chemicals

RPMI 1640 medium was obtained from Nissui Pharmaceutical Co., Ltd. (Tokyo, Japan), and fetal bovine serum (FBS) was obtained from Equitech-Bio, Inc. (Kerrville, TX, USA). Opti-modified Eagle's medium (Opti-MEM) was purchased from Thermo Fisher Scientific K.K. (Tokyo, Japan). All other chemicals were of the highest grade available and used without further purification.

2.2.2 ODNs

All ODNs used were purchased from Integrated DNA Technologies, Inc. (Coralville, IA, USA). The sequences of the ODNs are listed in Table 3. The ODNs were named Tet(idn)-01-04, where n refers to the number of common bases in the palindrome sequence and 01-04 represent different ODNs that form a tetrapodna. For the cellular uptake experiments, 5' fluorescently labeled tetrapodnas were prepared using Alexa Fluor 488-labeledTet(sym)-01 and Tet(id12)-01, which were purchased from Japan Bio Services Co., Ltd. (Saitama, Japan).

2.2.3 Preparation of tetrapodna

Each tetrapodna was prepared by annealing equimolar amounts of ODNs as previously described [41].

2.2.4 Cell culture

Murine macrophage-like cells, RAW 264.7, were cultured in RPMI 1640 medium supplemented with 10% heatinactivated FBS, 0.15% sodium bicarbonate, 100 units/mL penicillin, 100 mg/mL streptomycin, and 2 mM L-glutamine at 37°C and in humidified air containing 5% CO_2. Cells were then seeded on 48-well plates at a density of 5×10^5 cells/mL and cultured for 24 h prior to use.

2.2.5 Polyacrylamide gel electrophoresis (PAGE) analysis

All the samples were run on 6% polyacrylamide gels at 200 V for 30 min at 4°C and stained using ethidium bromide (Wako Pure Chemical Industries, Ltd.). The 20 bp DNA ladder was purchased

from Watson (Tokyo, Japan).

2.2.6 Measurement of melting temperature (Tm)

The thermal melting curve was obtained by measuring the absorbance of all the tetrapodna preparations in a Tris-EDTA (TE) buffer solution (10 mM Tris, 1 mM EDTA, pH 8) containing 150 mM sodium chloride and using a Shimadzu UV-1600 PC spectrometer (Kyoto, Japan) equipped with a TMSPC-8 temperature controller at 260 nm wavelength [65]. The thermal melting curve thus obtained was analyzed using the derivative method in order to calculate the melting temperature.

2.2.7 Small angle X-ray scattering (SAXS)

The SAXS measurements were performed at 25 °C using the BL40B2 at SPring-8 in Japan, in accordance with the method reported by Sanada *et al.* [31]. Samples were packed into a quartz capillary cell (Hilgenberg GmbH, Malsfeld, Germany) with a light path of 2 mm. The incident X-ray wavelength λ was fixed at 0.1 nm, and the distance between the samples and the detector's 30 cm × 30 cm imaging plate (Rigaku R-AXIS VII) was 2 m. This setup provided a q range from 0.1 to 6.0 nm^{-1}, where q is defined as $q = 4\pi \sin\theta/\lambda$ with a scattering angle of 2θ. In order to determine the excess scattering intensity of the DNAs, the background scattering of the buffer and the cell were subtracted after correction for the appropriate transmittance. When DNA solution was diluted to less than 3 mg/mL, the interparticle interferences [S(q)] could be ignored [59]; I therefore presumed that S(q) = 1 in the relationship $I(q) \approx S(q)P(q)$, where S(q) and P(q) are the structural and form factors, respectively.

2.2.8 Calculation of scattering intensity by modeling

Scattering intensity can be expressed as a Fourier transformation of the pair correlation function, p(r), of the scattering objects, where r is the distance between scattering points as previously reported [31]. For monodisperse particles, depending on their size and shape and without the interparticle interferences, the scattering intensity, I(q) can be expressed as follows:

$$I(q) \propto \int p(r)(\sin qr/qr)\, dr \quad (1)$$

This expression means that once p(r) is given, I(q) is obtained using the numerical calculation in eq 1. For the calculation of p(r), I used a rigid multirod model in which the rods had a uniform electron density [59]. Moreover, the cross-sectional area of the rod was neglected, and the rods were connected at one end. The angle at the connecting point could be changed.

2.2.9 Uptake of tetrapodna by RAW264.7 cells

RAW264.7 cells were seeded on 48-well plates at a density of 5×10^4 cells/well and incubated for 24 h before treatment. Then, the cells were treated with 100 nM Alexa Fluor 488-labeled tetrapodna

diluted with Opti-MEM for 2 h at 37 °C. The cells were then washed twice with phosphate buffered saline (PBS) and harvested. Subsequently, mean fluorescence intensity (MFI) of the cells was determined using a flow cytometer (FACS Calibur, BD Biosciences, NJ, USA). Data were analyzed using CellQuest software (version 3.1, BD Biosciences).

Table 3. The sequences of ODNs used for tetrapodna preparations.

Name	Sequences (5′ → 3′)	Length (mer)
Tet(sym)-01*	GCTAGACGTTCGATACCT AGCTAAGGTAGCTCTAGC	36
Tet(sym)-02	GCTAGAGCTACCTTAGCT TCCATACGTTGCAGAACC	36
Tet(sym)-03	GGTTCTGCAACGTATGGA TGCATTGCATCGAGATGC	36
Tet(sym)-04	GCATCTCGATGCAATGCA AGGTATCGAACGTCTAGC	36
Tet(id8)-01	GCTAGACGTTCGATAGCA TGCTAAGGTAGCTCTAGC	36
Tet(id8)-02	GCTAGAGCTACCTTAGCA TGCTTACGTTGCAGAACC	36
Tet(id8)-03	GGTTCTGCAACGTAAGCA TGCTTTGCATCGAGATGC	36
Tet(id8)-04	GCATCTCGATGCAAAGCA TGCTATCGAACGTCTAGC	36
Tet(id12)-01	GCTAGACGTTCGATAGCA TGCTATGGTAGCTCTAGC	36
Tet(id12)-02	GCTAGAGCTACCATAGCA TGCTATCGTTGCAGAACC	36
Tet(id12)-03	GGTTCTGCAACGATAGCA TGCTATGCATCGAGATGC	36
Tet(id12)-04	GCATCTCGATGCATAGCA TGCTATCGAACGTCTAGC	36
Tet(id16)-01	GCTAGACGTTCGATAGCA TGCTATCGTAGCTCTAGC	36
Tet(id16)-02	GCTAGAGCTACGATAGCA TGCTATCGTTGCAGAACC	36
Tet(id16)-03	GGTTCTGCAACGATAGCA TGCTATCGATCGAGATGC	36
Tet(id16)-04	GCATCTCGATCGATAGCA TGCTATCGAACGTCTAGC	36
Tet(asym12)-01*	GCTAGACGTTCGATACCTAGCTAA GGTAGCTCTAGC	36
Tet(asym12)-02	GCTAGAGCTACC AATGCATCCATACGTTGCAGAACC	36
Tet(asym12)-03	GGTTCTGCAACGTATGGATGCATT CCATCGAGATGC	36
Tet(asym12)-04	GCATCTCGATGG TTAGCTAGGTATCGAACGTCTAGC	36
Tet(asym16)-01*	GCTAGACGTTCGATACCTAGCTAAGG TAGCTCTAGC	36
Tet(asym16)-02	GCTAGAGCTA GCAATGCATCCATACGTTGCAGAACC	36
Tet(asym16)-03	GGTTCTGCAACGTATGGATGCATTGC ATCGAGATGC	36
Tet(asym16)-04	GCATCTCGAT CCTTAGCTAGGTATCGAACGTCTAGC	36

All ODNs have a phosphodiester backbone.
* Tet(sym) 01, Tet(asym12) 01 and Tet(asym16) 01 have the same sequences.

2.3 Results and Discussion

2.3.1 Design of tetrapodnas with different structural

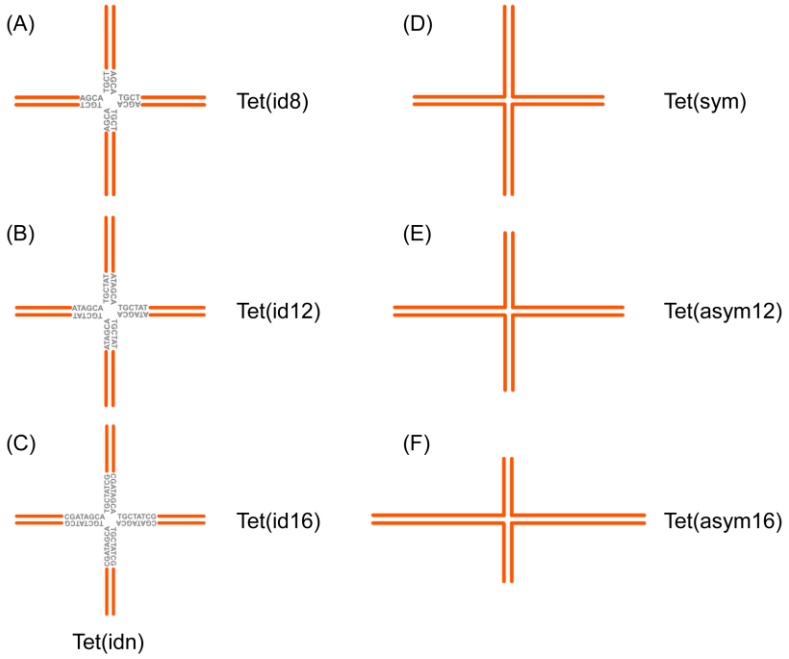

Figure 8. Schematic representation of the putative structures of tetrapodna consisting of four ODNs. (A−C) Tet(idn), the gray letters at the center of tetrapodna represent identical palindrome sequences of different lengths; n indicates the number of bases in the palindrome sequence. (D) Tet(sym), symmetric conformation with fully complementary sequences. (E, F) Tet(asym), asymmetric conformation with fully complementary sequences, the number in brackets indicates the difference between the length of the long arm and that of the short arm in a tetrapodna conformation.

Our previous study demonstrated that tetrapod-like structures can be completely formed by annealing four corresponding ODNs [30]. Figure 8 shows the schematic presentation of the six types of tetrapodna designed in this study. Tet(sym), which is identical to the tetrapodna reported in the previous study [13], can adopt only the structure symmetric with four 18 base-long double stranded pods. Tet(asym16) can only adopt the structure asymmetric with two 10 base-long and two 26 base-long double stranded pods. Similarly, Tet- (asym12) has two 12 base-long and two 24 base-long double stranded pods as shown in the figure. In addition, Tet(id8), Tet(id12), and Tet(id16) were designed by replacing the central sequence of Tet(sym) with either 8-, 12-, or 16-base long palindrome sequences, respectively. Theoretically, these tetrapodnas with palindrome sequences can adopt either symmetric or asymmetric conformation. Specifically, Tet(id12) can adopt a tertiary structure that is identical to Tet(sym) or Tet(asym12) or a structure that is something between these two.

2.3.2 Formation of the tetrapodnas

Four kinds of 36-mer ODNs were annealed to construct each tetrapodna. In order to confirm whether the tetrapodnas were formed as I designed, I carried out PAGE analysis. The analysis indicated that all the tetrapodna preparations were abundantly formed except for Tet(asym16) (Figure 9). Tet(asym16) was not completely obtained in a tetrapod-like shape; instead a smear was formed due to the instability at room temperature after the annealing operation. In addition, the single strand ODNs

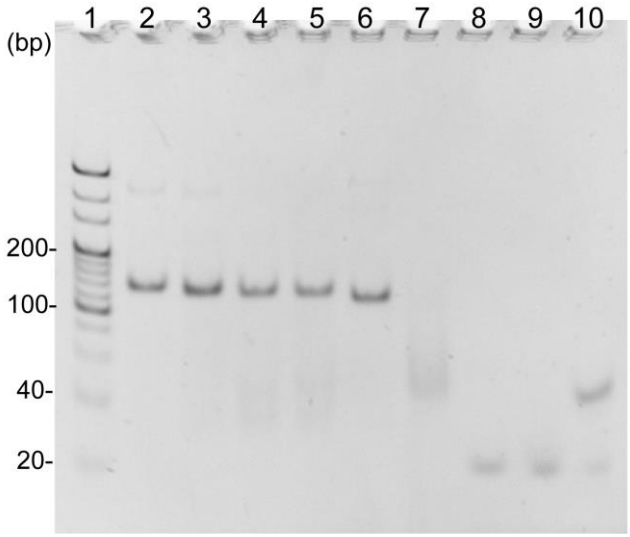

Figure 9. PAGE analysis of tetrapodna preparations. Each sample was run on a 6% polyacrylamide gel at 200 V for 30 min at 4°C. Lane 1, 20 bp DNA ladder; lane 2, Tet(sym); lane 3, Tet(id8); lane 4, Tet(id12); lane 5, Tet(id16); lane 6, Tet(asym12); lane 7, Tet(asym16); lane 8, Tet(sym) 01; lane 9, Tet(id8) 01; lane 10, Tet(id12) 01.

with 12-base palindrome sequences, Tet(id12)-01, showed a shorter migration distance than Tet(sym)-01, the one without palindrome sequence, suggesting that Tet(id12)-01 formed homoduplex preferentially compared to the ones without palindrome sequences.

Owing to the superiority of DNA nanoparticles as a powerful and functional biomaterial [8-11], some 3D-DNA nanostructures that revealed high biological efficiency have been reported in previous studies [30, 32, 34]. By assembling ODNs in an ordered conformation such as tetrapodna [41], a B-form DNA had been verified using spectral characteristics in our former research [59]. The PAGE analysis of Tet(asym12), an asymmetric tetrapodna, exhibited a slightly but not significantly longer migration distance than the others, probably due to higher asymmetry properties than that of Tet(id12). The formation of a smear of Tet(asym16) suggested that the shorter double strands consisting of 10-base pairs were too short for stable tetrapod-like structure formation. Therefore, I selected the well-formed Tet(asym12) and its corresponding Tet(id12) with palindrome sequence as representative tetrapodnas in the present study because Tet(asym12) had the most asymmetric features among those efficiently formed.

2.3.3 Thermal stability

Table 4 summarizes the Tm values of the tetrapodnas. Tet(id12), the flexible one, had a little higher Tm value than other DNA structures. However, the Tm values were comparable to one another. Figure 10 shows the melting curves of the tetrapodnas. A sharp increase in the melting curve of Tet(sym) around 65°C indicated a one-stage dissociation process. In contrast, there were two-stage increases in the curve of Tet(asym12), which had two 12 base and two 24 base long double stranded pods. The shape of the melting curve of Tet(id12) was close to that of Tet(asym12) but not to that of Tet(sym), indicating that Tet(id12) also had a two-step dissociation process.

Sample	Tm (°C)
Tet(sym)	64.0
Tet(id8)	67.9
Tet(id12)	70.5
Tet(asym12)	67.5

Table 4. Melting temperatures (Tm) of tetrapodna preparations. Tm was calculated from the thermal melting curves of tetrapodna preparations in a TE buffer solution (pH 8) containing 150 mM sodium chloride, using the derivative method.

Given the typical features of palindrome sequences, more concise tetrapodna structures have been constructed by introducing the same palindrome sequences into the ODNs. The discrepancy in Tm values between the tetrapodna with a symmetric conformation and one with an asymmetric conformation indicates the different dissociation processes. The melting curve of Tet-(sym) exhibited

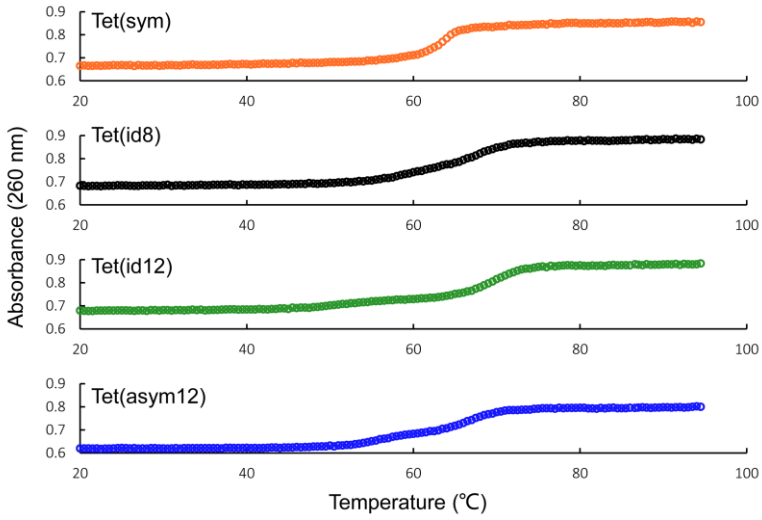

Figure 10. Thermal melting curves of tetrapodna preparations obtained by heating gradually from 0 to 95°C at a constant rate of 1 °C/min. The temperature variation between each measuring point was 0.5°C.

a sharp increase, thus revealing a one-stage dissociation process. In contrast to the characteristics of Tet(sym), Tet(asym12) exhibiting an apparent two-stage process in the melting curve demonstrating that the 12 base-long double stranded parts dissociate at a lower temperature than the 24 base-long parts. The dissociation process of Tet(id12) was similar to that of Tet(asym12), thus indicating that Tet(id12) was dissolved in an approximate double-stranded intermediate conformation first, and then the intermediate was melted into single-strand. In addition, Tet(id12) which had a melting temperature higher than that of Tet(sym) and similar to that of Tet(asym12) also confirmed the two-stage feature in the dissociation process.

2.3.4 X-ray scattering

SAXS analysis was carried out based on the assumptions mentioned above to evaluate the constructional differences between the tetrapodna structures without palindrome sequences and palindromic tetrapodna structures. Figure 11 shows the scattering profiles of each type of tetrapodna.

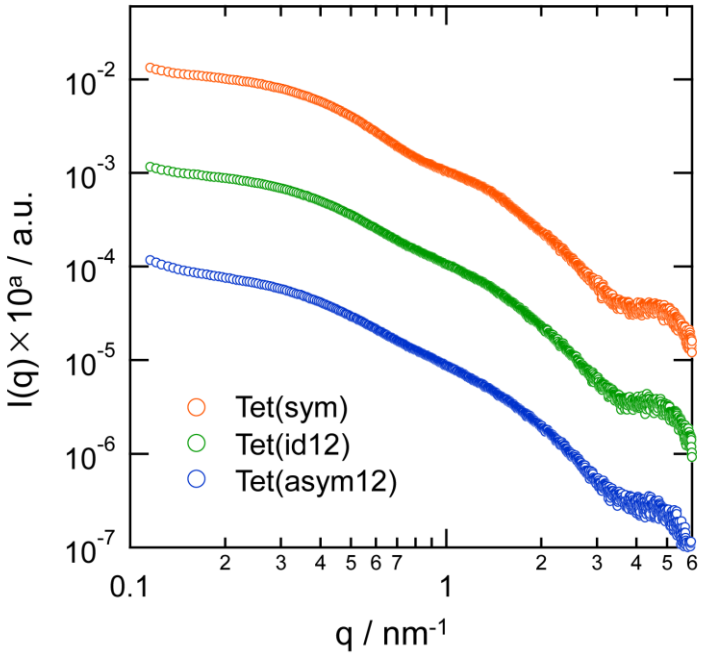

Figure 11. SAXS profiles of Tet(sym), Tet(id12) and Tet(asym12). All measurements were performed in a Tris-EDTA (TE) buffer solution (10 mM Tris, 1 mM EDTA, pH 8) containing 150 mM sodium chloride at 25°C.

Though all scattering profiles seemed to be almost identical, a very small difference among their oscillation behavior at q = 0.7 to 1.0 nm^{-1} could be observed. While the SAXS profile of Tet(asym12) exhibited negligible oscillation in the q range, Tet(sym) displayed slightly stronger oscillation compared to that of the others. The oscillation in the q range reflected the symmetric structure of tetrapodna, which was also indicated by the SAXS simulation of theoretical curves shown in Figure 12. This figure represents the symmetric and asymmetric tetrapodnas, respectively, using the rigid

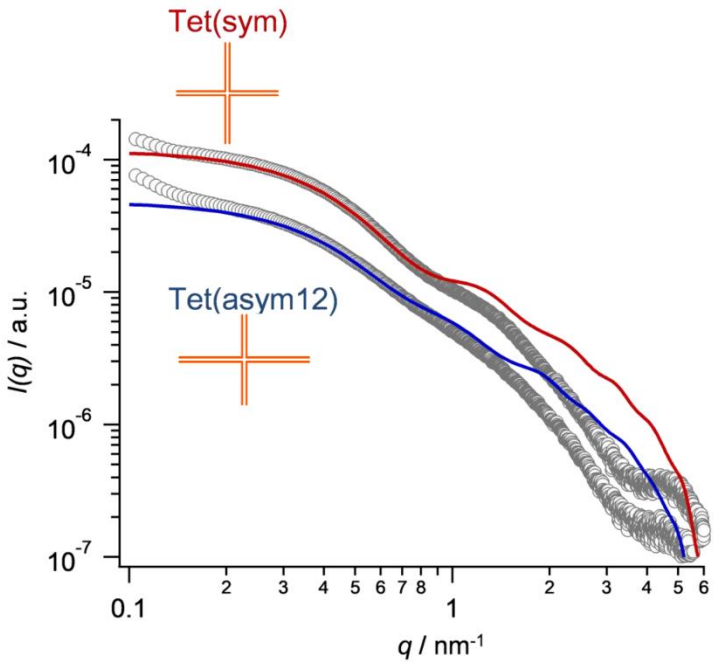

Figure 12. SAXS profiles of experimental data and theoretical curves using the rigid four-rod model.

four-rod models. According to the SAXS simulation, a more symmetric tetrapodna exhibited a stronger oscillation than a less symmetric one. In addition, the experimental data of Tet(sym) and Tet(asym12) were also compared with theoretical curves, and the results indicate that the theoretical models can successfully reproduce the SAXS profiles of Tet(sym) and Tet(asym12) up to a limited q-range, from 0.2 to 0.9 nm^{-1}. The oscillation in the profile of Ted(id12) was closer to that of Tet(sym) than to that of Tet(asym12) in SAXS profiles, indicating the formation of a symmetric tetrapodna structure due to the flexibility of palindrome sequences in the center.

Guinier plots of ln[I(q)] versus q^2 of the tetrapodnas are given in Figure 13 and Table 5. The

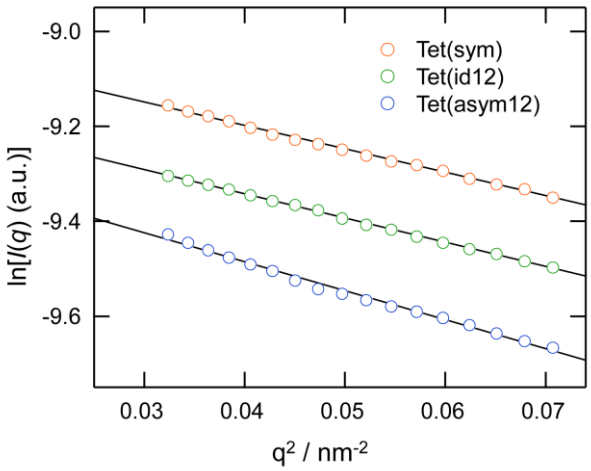

Figure 13. Guinier plots (i.e., ln*I*(*q*)/*c* versus q^2)) of Tet(sym), Tet(id12) and Tet(asym12).

gyration radii (Rg) of Tet(sym), Tet(id12), and Tet(asym12) were determined to be 3.85, 3.91, and 4.27 nm, respectively. The theoretically calculated Rg values for Tet(sym) and Tet(asym12) are 3.68

and 4.22 nm, respectively, and those values were almost consistent with the ones estimated using the Guinier plots. Note that the Rg of Tet(id12) was closer to that of Tet(sym) compared to that of Tet(asym12), strongly indicating that Tet(id12) was more inclined to adopt a symmetric structure similar to that of Tet(sym) in the solution spontaneously.

Table 5. Radii of gyration of tetrapodna preparations determined by Guinier plots and calculated values.

Sample	$R_{g\_expt.}$ / nm	$R_{g\_calc.}{}^{a}$ / nm
Tet(sym)	3.85 ± 0.05	3.68
Tet(id12)	3.91 ± 0.05	—
Tet(asym12)	4.27 ± 0.12	4.22

[a] R_g was calculated using the equation; $R_g^2 = \sum_{i=0}^{N} r_i^2/(N+1)$ where N is the number of scattering points and r is the distance between the mass center of the tetrapodnas and the position of each base pair. Distance between base pairs was assumed as 0.340 nm in the calculation.

Our previous studies demonstrated that the X-shaped preparation, or tetrapodna, was assembled as a tetrapod shape [30, 49]. A more detailed description about the formation of a tetrapod-like three-dimensional conformation, not a two-dimensional one, in aqueous solution has been made by using synchrotron X-ray scattering experiments, in which four kinds of theoretical models with different angles at the junction of tetrapodna were compared [59]. The junction at which the four equivalent pods of tetrapodna were connected was assumed to be flexible. On the other hand, the arms or pods of the tetrapodna, which consist of short double strand DNA, were considered as rigid parts because of their short length [66]. In addition, the low q region of SAXS profile reflects the global structure of the tetrapodna, and the local structure of the particles does not affect that region [31]. As shown in Figure 12 in which the experimental data were compared with theoretical curves, the rigid four-rod model could successfully reproduce the SAXS profiles of Tet(sym) and Tet(asym12) up to a limited q-range: from 0.2 to 0.9 nm^{-1}. The high q region of SAXS profile is related to the autocorrelation function to resolve how the electron densities separated by 2−6 nm are correlated to each other. Therefore, the discrepancy between the models and the data is ascribed to neglect of the diameter or lateral structures in the four-rod models [59]. Therefore, the individual arms of the tetrapodna could be regarded as rigid rods. Based on these results, I used a geometrical multirod model in this thesis.

Furthermore, another group reported that the 4-arm branched DNA molecules with identical arm length preferred to adopt an asymmetric distorted-X shape [60]. However, to my knowledge, there

is no related report about tetrapodnas with identical palindrome sequences at the center of the structure so far. Therefore, I believe that it is appropriate to discuss the overall spread of the macromolecules by comparing the value of the radius of gyration. The SAXS profiles revealed that Tet(id12) adopted either a similar symmetric structure or a structure that was a mixture of Tet(sym) and Tet(asym12) in solution. There are some difficulties in distinguishing the SAXS profiles of these two situations. Based on the PAGE result, which displayed only one clear band, it is most probable that Tet(id12) adopts a similar symmetric conformation at temperatures much below the Tm. On the other hand, when the temperature increased, Tet(id12) started to dissociate into single strands in a two-step procedure. According to the melting curve of Tet(id12), which was similar to that of Tet(asym12), Tet(id12) would form an asymmetric structure similar to Tet(asym12) at temperatures around the Tm. Taken together, these results suggested that Tet(id12) had a similar structure to Tet(sym) at low temperatures below the Tm and it dissociated into substructures whose structural properties were similar to those of Tet(asym12) at higher temperatures. Recently, Bruetzel *et al.* successfully observed the dynamic structures of a DNA origami switch by using time-resolved SAXS [67]. A more structured specification of the nanostructured DNA is expected to be explored soon by SAXS.

2.3.5 Cellular uptake evaluation of X-shaped DNA

Figure 14 indicates the MFI values of RAW264.7 cells after addition of Alexa Flour 488-labeled tetrapodnas or a linear single strand DNA (ssDNA). All the tetrapodnas showed higher MFI values than the negative control (Opti-MEM) or ssDNA, whereas there were no significant differences among all the tetrapodnas. In a study from my laboratory [31], a difference in Rg values of about 0.5

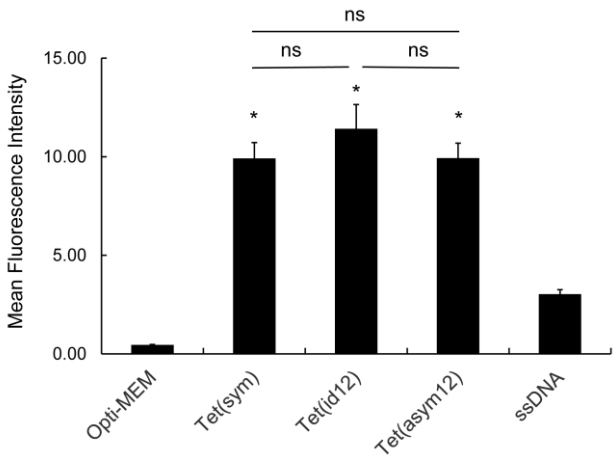

Figure 14. Uptake of tetrapodna preparations and ssDNA by RAW264.7 cells. Each Alexa Fluor 488-labeled DNA sample was added to cells at a final concentration of 0.1 μM in Opti-MEM, and cells were incubated for 2 h at 37°C. The samples associated with cells were quantified using flow cytometry, and the MFI was calculated in order to compare the cellular uptake of each preparation. Tet(sym)-01, one of the ODNs for Tet(sym), was used as ssDNA. Results are expressed as the mean ± SD of four measurements. *P < 0.01 compared with the Opti-MEM alone group, ns = not significant.

significantly affected the cellular uptake of polypod-shaped DNAs by RAW264.7 cells. In contrast, a similar difference hardly affected the uptake efficiency of the tetrapodnas in the present study. These

results demonstrated that the uptake efficiency was hardly affected by the symmetricity of the tetrapodnas.

In addition to determining the structural properties of tetrapodna, the biological evaluation of these structures is indispensable in the application of tetrapodna as a prominent biomaterial. Studies from my research group using various types of DNA nanostructures demonstrated that the interaction of DNA nanostructures and cells was mainly determined by their tertiary structural features. It was undefined before this study whether the global structure of DNA nanostructures, such as the symmetricity, affected their cellular interactions. In the present study, I showed that the palindrome sequence could cause different conformation that a DNA nanostructure took. Based on the cellular uptake results obtained in this manuscript, I conclude that the uptake efficiency is hardly affected by the symmetricity of the tetrapodnas. This discrepancy from the previous results would be explained by the fact that the differences in their structural properties, such as size, among the tetrapodnas used in this study were smaller than those in previous studies.

With numerous DNA biological materials coming to the fore, quality assurance and biological safety should be emphasized for the development of nucleic acid medicines [68-70]. The use of identical palindrome sequence provides a couple of advantages. First, designing the sequence is a complicated process in the construction of polypod-like structured DNA. The parts of identical palindrome sequence can be repeatedly used in designing other DNA nanostructures. Second, the biological activities, including toxicity and immunostimulatory activity, are dependent mainly on the sequence. The use of palindrome sequence greatly reduces the number of different sequences as well as the possibility of off-target effects caused by hybridization or other unintentional effects [61, 62, 71, 72]. Lastly, the Tm measurement revealed that Tet(id12) had a higher Tm value than ones without palindrome sequences (Table 4), indicating that palindrome sequence can increase the structural stability of DNA nanostructures. Therefore, the construction of DNA nanoparticles that are more purified and controllable is imperative and more research on ODN sequences will be necessary in the future.

Chapter 3　Elucidation of the effect of the position of CpG motif in polypod-like structured DNA on immune stimulation.

（多足型 DNA 構造体中の CpG motif の位置が免疫活性化に及ぼす影響の解明）

3.1 Introduction

The CpG motif consists of an unmethylated cytosine-guanine dinucleotide with appropriate flanking sequences, namely, ligand of Toll-like receptor-9 (TLR9). DNA or synthetic oligodeoxynucleotides (ODNs) containing this motif induce pro-inflammatory cytokine responses in TLR9-positive cells [73-75]. Synthetic CpG ODNs can be classified into five types [76]; each type has unique structural and functional characteristics [77-79]. The optimal sequences for CpG motifs vary among species, and the optimal sequences for rodents and humans have been determined as GACGTT and GTCGTT, respectively.

A recent study indicated that TLR9 recognizes the CpG motif in a single-stranded form [83]. Ohto *et al.* reported the integrated crystal structures of TLR9 with agonistic CpG DNA and elucidated the existence of a symmetric TLR9–CpG DNA complex with 2:2 stoichiometry when an agonistic CpG DNA was bound to TLR9 [58]. This research group also found that TLR9 had two DNA-binding sites: one for CpG DNA and the other for DNA containing cytosine at the second position from the 5'-end [57]. This additional binding site could stabilize the TLR9–CpG DNA complex. Furthermore, this additional binding site outside the CpG motif may provide an explanation for the differences in biological activities, including inflammatory cytokine release [80-82].

CpG ODNs are expected to be used as adjuvants to stimulate the innate immune system [1, 83]. ODN1018, a phosphorothioate-stabilized CpG ODN, is included in Heplisav-B, a hepatitis B vaccine approved by the US FDA [86]. It has been reported that high doses of phosphorothioate-stabilized ODNs are nephrotoxic [87]. Therefore, one of the challenges in the development of CpG ODNs for clinical use is the design of CpG ODNs with strong immunostimulatory activity and low toxicity. As described above, the activity of CpG ODN is related to the sequence of both the CpG motif and other parts of the ODN, and various rules have been proposed [57, 58, 80-82]. However, these rules were derived from the results of single-stranded ODNs, and little is known about how the sequences of the ODNs constructing three-dimensional nanostructures affect the immune responses of TLR9-positive cells.

In Chapters 1 and 2, I have explored the structural properties of polypodnas when the structures were flattened under unconstrained conditions (Chapter 1) or in solution (Chapter 2). The results on the immunostimulatory activity of polypodnas showed that the complicated structures of polypodnas were linked with efficient uptake by TLR9-positive immune cells, followed by high production of cytokines. However, few attempts have been made to examine the effect of the sequences of ODNs constructing polypodnas. The optimization of the sequence will further increase the potency of CpG motif-containing polypodnas as an immune adjuvant. Therefore, in Chapter 3, I

have tried to optimize the sequence of the CpG ODNs that construct the polypodnas. To this end, four types of CpG ODNs with a potent CpG motif at varying positions in the sequence were designed. In addition, polypodnas can be designed to form structures with only double-stranded parts or with both single- and double-stranded parts. Therefore, polypodna with the CpG motif either in the double-stranded part or single-stranded part was designed to examine whether this difference affected cytokine release after the addition of the CpG motif containing polypodna to TLR9-positive immune cells. Each CpG ODN was used to construct tripodnas (three pods), tetrapodnas (four pods), pentapodnas (five pods), and hexapodnas (six pods). The formation of these polypodnas was confirmed by polyacrylamide gel electrophoresis (PAGE), and the melting temperature (Tm) was measured. Subsequently, the uptake and cytokine release after incubation with RAW264.7 cells were investigated, and the effect of the location of the CpG motif in the CpG ODN on these parameters was evaluated.

3.2 Materials and Methods

3.2.1 Chemicals

RPMI1640 medium was obtained from Nissui Pharmaceutical Co., Ltd. (Tokyo, Japan), and fetal bovine serum (FBS) was obtained from Equitech-Bio, Inc. (Kerrville, TX, USA). Opti-modified Eagle's medium (Opti-MEM) was purchased from Thermo Fisher Scientific K.K. (Tokyo, Japan). All other chemicals were of the highest grade available and were used without further purification.

3.2.2 ODNs

All ODNs used were purchased from Integrated DNA Technologies, Inc. (Coralville, IA, USA). The sequences of the ODNs are listed in Table 6. Each ODN was named, in a form such as CpG-std Hex01, with a series name of std, core, ext(out), or ext(in), shape (hexa, penta, tetra, tri, ds), and ODN number (1-6). The ODNs assigned number 1, such as CpG-std hexa1, contained a potent CpG motif and cytosine at the second position from the 5'-end. For the cellular uptake experiments, 5'-fluorescently labeled versions of each polypodna were prepared by using Alexa Fluor 488-labeled CpG-std hexa1, CpG-core hexa1, CpG-ext(out) hexa1, and CpG-ext(in) hexa1, which were purchased from Japan Bio Services Co., Ltd. (Saitama, Japan). For the TNF-α release and cellular uptake experiments following sequential administration, 3'-fluorescently labeled versions of each tetrapodna was prepared by using Alexa Fluor 488-labeled CpG-ext(out) hexa1 and CpG-ext(in) hexa1, which were purchased from Japan Bio Services Co., Ltd. (Saitama, Japan).

3.2.3 Preparation of polypodna

Each ODN was prepared at a final concentration of 0.1 mM in 150 mM sodium chloride buffer. All polypodna samples were prepared in 150 mM sodium chloride buffer by annealing equimolar volumes of ODN solutions. The mixtures were incubated at 95°C for 5 min and cooled down to 65°C for 2 min by using a thermal cycler. Subsequently, the mixtures were cooled to 62°C for 2 min at a rate of 0.6°C/min, and then cooled to 4°C at a rate of 2°C/min [36].

3.2.4 Cell culture

The murine macrophage-like cells, RAW264.7, were cultured in RPMI1640 medium supplemented with 10% heat-inactivated FBS, 0.15% sodium bicarbonate, 100 units/mL penicillin, 100 mg/mL streptomycin, and 2 mM L-glutamine at 37°C in humidified air containing 5% CO_2. The cells were then seeded on 96-well or 48-well plates at a density of 5×10^5 cells/mL and cultured for 24 h prior to use.

3.2.5 Polyacrylamide gel electrophoresis

The samples were separated on 6% polyacrylamide gels at 200 V for 20 min at room temperature and stained with SYBR Gold (Molecular Probes, Eugene, OR, USA). The 20 bp DNA ladder was purchased from Watson (Tokyo, Japan).

3.2.6 Measurement of melting temperature

The thermal melting curve was obtained through the measurement of the absorbance of all the polypodna preparations in 150 mM sodium chloride buffer solution by using a quartz cell with a 1 mm optical path length (JASCO, Tokyo, Japan) with a spectrophotometer (JASCO J-730, JASCO) at 260 nm. All samples were measured while heating from 20°C to 95°C at a rate of 0.5°C/min and the absorbance was recorded at 1.0°C. The thermal melting curves obtained were analyzed by using the conventional two-point average method to obtain the Tm.

3.2.7 TNF-α release from RAW264.7 cells

RAW264.7 cells were seeded in 96-well plates at a density of 5×10^4 cells/well and incubated for 24 h before treatment. Then, ssDNA, dsDNA, or each type of polypodna (100 nM in Opti-MEM) were added to the cells. The cells were incubated for 8 h, and the supernatants were collected and stored at −80°C until use. For the time-course study, the supernatants were collected at 0.5 h, 1 h, 2 h, and 4 h after addition of DNA samples. The levels of TNF-α in the supernatants were determined by enzyme-linked immunosorbent assay in accordance with the manufacturer's protocol (BioLegend, Inc., San Diego, CA, USA).

3.2.8 Uptake of tetrapodna by RAW264.7 cells

RAW264.7 cells were seeded in 48-well plates at a density of 1 × 10^5 cells/well and incubated for 24 h before treatment. The cells were then treated with Alexa Fluor 488-labeled polypodna (100 nM in Opti-MEM) for 2 h at 37°C. For the time-course study, the cells were treated with Alexa Fluor 488-labeled polypodna (100 nM in Opti-MEM) for 0.5 h, 1 h, 2 h, and 4 h at 37°C. The cells were then washed twice with phosphate buffered saline (PBS) and harvested. Subsequently, the mean fluorescence intensity (MFI) of the cells was determined by using a flow cytometer (FACS Calibur, BD Biosciences, NJ, USA). The data were analyzed using CellQuest software (version 3.1, BD Biosciences) or FlowJo software (version 8.8.4; Beckman Coulter).

Table 6. The sequences of ODNs used for polypodna preparations.

Name	**Sequences (5′ → 3′)**	**Length (base)**	**Pod number**				
			6	**5**	**4**	**3**	**2**
CpG-std							
Std ODN#1	GCTAGACGTTCCATACCT GACTAAGCTAGCTCTAGC	36	✓	✓	✓	✓	✓
Std ODN#2	GCTAGAGCTAGCTTAGTC TCCATAGGTTGCAGAACC	36	✓	✓	✓	✓	
Std ODN#3	GGTTCTGCAACCTATGGA TGCATTGCATGCAGATGC	36	✓	✓	✓		
Std ODN#4	GCATCTGCATGCAATGCA CTCATAGCAAGCAGATGC	36	✓	✓			
Std ODN#5	GCATCTGCTTGCTATGAG AGCATTGGTAGCAGAACC	36	✓				
Std ODN#6	GGTTCTGCTACCAATGCT AGGTATGGAACGTCTAGC	36	✓				
Std ODN#7	GCATCTGCTTGCTATGAG AGGTATGGAACGTCTAGC	36		✓			
Std ODN#8	GCATCTGCATGCAATGCA AGGTATGGAACGTCTAGC	36			✓		
Std ODN#9	GGTTCTGCAACCTATGGA AGGTATGGAACGTCTAGC	36				✓	
Std ODN#10	GCTAGAGCTAGCTTAGTC AGGTATGGAACGTCTAGC	36					✓
CpG-core							
Core ODN#1	GCTACCATCACTGACGTT GACTAAGCTAGCTCTAGC	36	✓	✓	✓	✓	✓
Core ODN#2	GCTAGAGCTAGCTTAGTC TCCATAGGTTGCAGAACC	36	✓	✓	✓	✓	
Core ODN#3	GGTTCTGCAACCTATGGA TGCATTGCATGCAGATGC	36	✓	✓	✓		
Core ODN#4	GCATCTGCATGCAATGCA CTCATAGCAAGCAGATGC	36	✓	✓			
Core ODN#5	GCATCTGCTTGCTATGAG AGCATTGGTAGCAGAACC	36	✓				
Core ODN#6	GGTTCTGCTACCAATGCT AACGTCAGTGATGGTAGC	36	✓				
Core ODN#7	GCATCTGCTTGCTATGAG AACGTCAGTGATGGTAGC	36		✓			
Core ODN#8	GCATCTGCATGCAATGCA AACGTCAGTGATGGTAGC	36			✓		
Core ODN#9	GGTTCTGCAACCTATGGA AACGTCAGTGATGGTAGC	36				✓	
Core ODN#10	GCTAGAGCTAGCTTAGTC AACGTCAGTGATGGTAGC	36					✓
CpG-ext(out)							
Ext(out) ODN#1	GCTAGACGTTCCTTTTTT GCTTCAGTTGCCATACCT GACTAAGCTAGCTCTAGC	54	✓	✓	✓	✓	✓
Ext(out) ODN#2	GCTAGAGCTAGCTTAGTC TCCATAGGTTGCAGAACC	36	✓	✓	✓	✓	
Ext(out) ODN#3	GGTTCTGCAACCTATGGA TGCATTGCATGCAGATGC	36	✓	✓	✓		
Ext(out) ODN#4	GCATCTGCATGCAATGCA CTCATAGCAAGCAGATGC	36	✓	✓			
Ext(out) ODN#5	GCATCTGCTTGCTATGAG AGCATTGGTAGCAGAACC	36	✓				
Ext(out) ODN#6	GGTTCTGCTACCAATGCT AGGTATGGCAACTGAAGC	36	✓				
Ext(out) ODN#7	GCATCTGCTTGCTATGAG AGGTATGGCAACTGAAGC	36		✓			
Ext(out) ODN#8	GCATCTGCATGCAATGCA AGGTATGGCAACTGAAGC	36			✓		
Ext(out) ODN#9	GGTTCTGCAACCTATGGA AGGTATGGCAACTGAAGC	36				✓	
Ext(out) ODN#10	GCTAGAGCTAGCTTAGTC AGGTATGGCAACTGAAGC	36					✓
CpG-ext(in)							
Ext(in) ODN#1	GCTTCAGTTGCCTTTTTT	54	✓	✓	✓	✓	✓

	GCTAGACGTTCCATACCT GACTAAGCTAGCTCTAGC						
Ext(in) ODN#2	GCTAGAGCTAGCTTAGTC TCCATAGGTTGCAGAACC	36	✓	✓	✓	✓	
Ext(in) ODN#3	GGTTCTGCAACCTATGGA TGCATTGCATGCAGATGC	36	✓	✓	✓		
Ext(in) ODN#4	GCATCTGCATGCAATGCA CTCATAGCAAGCAGATGC	36	✓	✓			
Ext(in) ODN#5	GCATCTGCTTGCTATGAG AGCATTGGTAGCAGAACC	36	✓				
Ext(in) ODN#6	GGTTCTGCTACCAATGCT AGGTATGGAACGTCTAGC	36	✓				
Ext(in) ODN#7	GCATCTGCTTGCTATGAG AGGTATGGAACGTCTAGC	36		✓			
Ext(in) ODN#8	GCATCTGCATGCAATGCA AGGTATGGAACGTCTAGC	36			✓		
Ext(in) ODN#9	GGTTCTGCAACCTATGGA AGGTATGGAACGTCTAGC	36				✓	
Ext(in) ODN#10	GCTAGAGCTAGCTTAGTC AGGTATGGAACGTCTAGC	36					✓

All ODNs have a phosphodiester backbone.

3.3 Results and Discussion

3.3.1 Structure of four series of polypodnas with different CpG motif position

My laboratory has previously demonstrated that a high yield of polypod-like structured DNA can be formed by annealing three to eight ODNs [30]. A schematic diagram of each series of polypodna with 3–6 pods designed in this study in this study is shown in Figure 15. In all cases, the double-stranded parts of all the pods consisted of 18 bases. The structures of the CpG-std series were identical to those of the CpG-core series, and these two series differed from each other with respect to the location of the CpG motif; the motif was close to the 5′ end of the ODN in the CpG-std series (Figure 15A), and the motif was near to the core (middle) region in the CpG-core series (Figure 15B). The CpG ODNs for CpG-ext(out) and CpG-ext(in), that is, Ext(out) ODN#1 and Ext(in) ODN#1, had a single-stranded part (an extension) at the 5′ end of the ODNs. The CpG-ext(out) series had the CpG

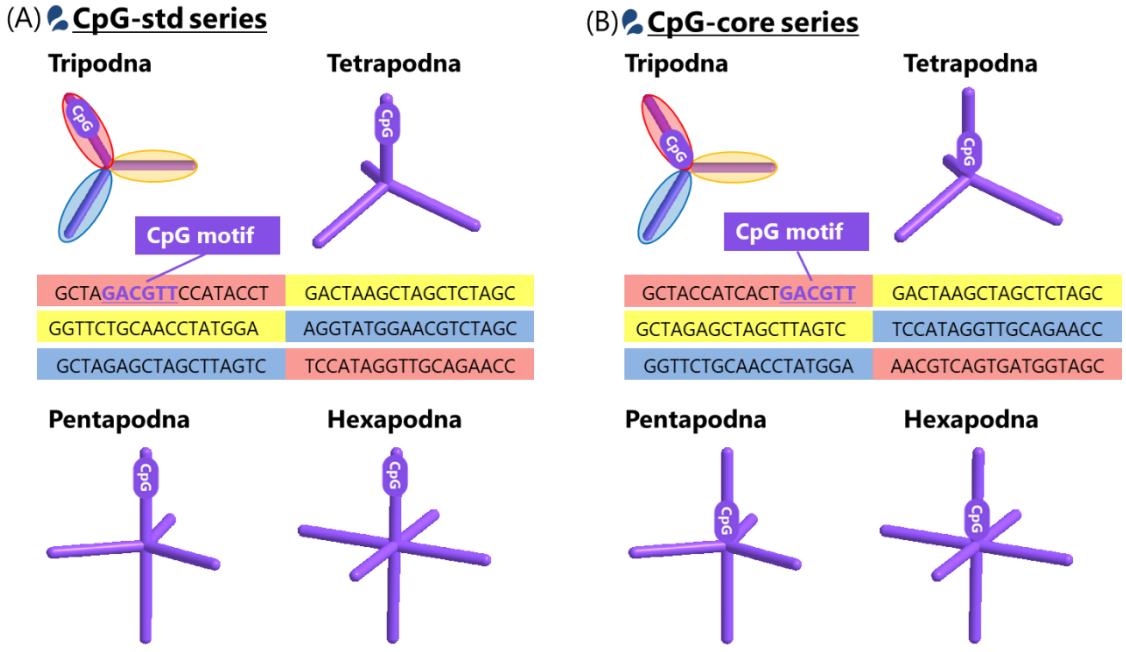

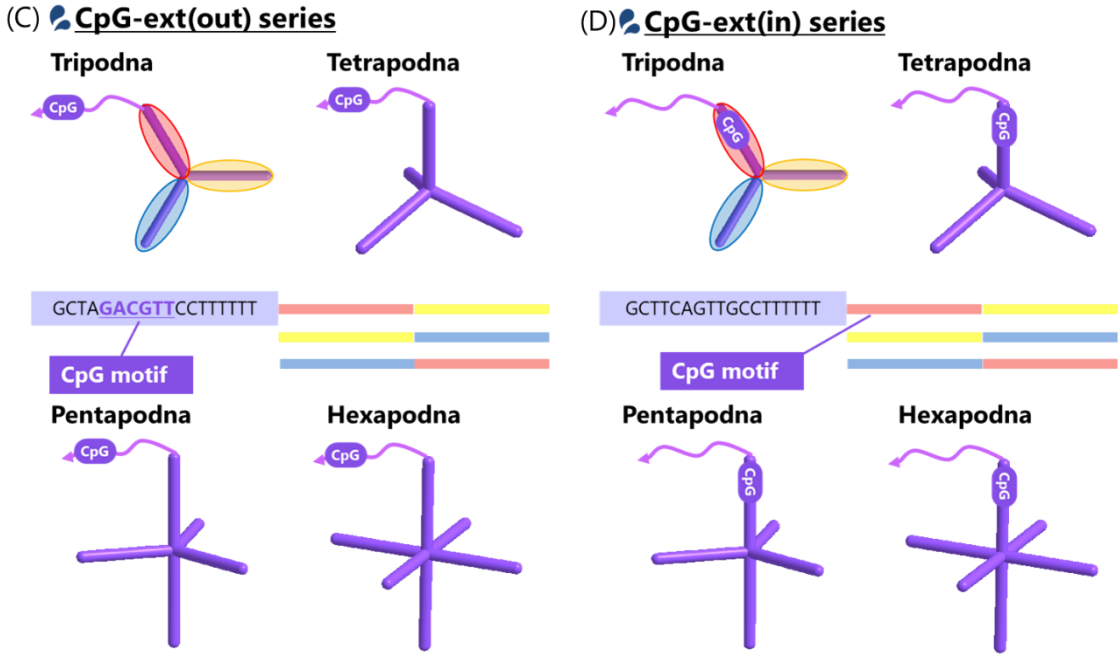

Figure 15. Schematic representation of the putative structures of polypodna series consisting of 3–6 ODNs: (A) CpG-std series, (B) CpG-core series, (C) CpG-ext(out) series, and (D) CpG-ext(in) series. The red, blue, and yellow colors indicate the complementary sequence between the same colors. The curved arrow represents the single-strand standing out of the polypodna structure. The CpG motif is marked in purple at different points in the polypodna structures.

motif in the single-stranded part (Figure 15C), whereas the CpG-ext(in) series had the motif in the double-stranded part (Figure 15D).

3.3.2 Formation and physicochemical properties of four series of polypodna

The formation of four series of polypodna was evaluated by PAGE. As shown in Figure 16, all the prepared polypodnas showed a single major band on the gel. In all the cases, the greater the pod number, the shorter the migration distance, indicating an increase in the size depending on the pod

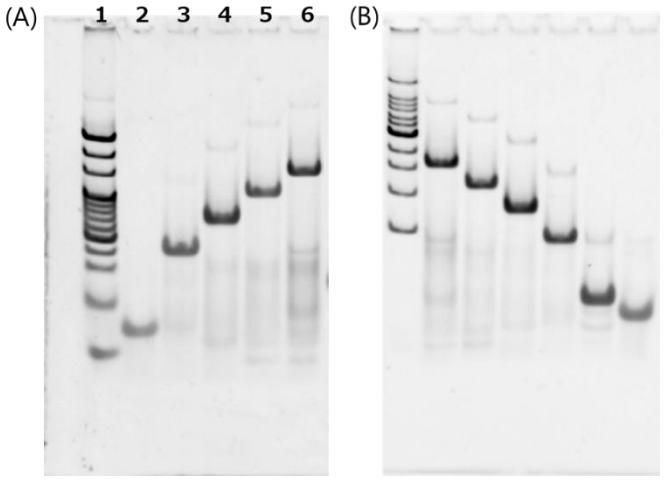

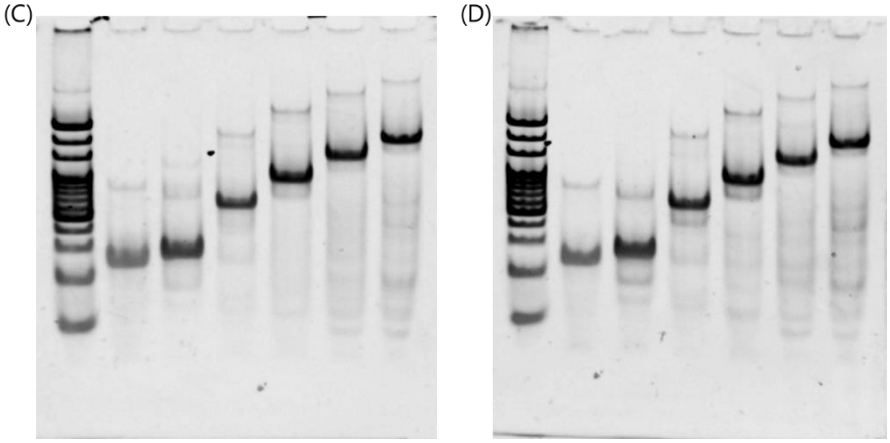

Figure 16. PAGE analysis of polypodna preparations. Each sample was separated on a 6% polyacrylamide gel at 200 V for 20 min at 4°C. (A) CpG-std series: Lane 1, 20 bp DNA ladder; lane 2, single-strand DNA; lane 3, tripodna; lane 4, tetrapodna; lane 5, pentapodna; lane 6, hexapodna. (B) CpG-core series: lane 1, 100 bp DNA ladder; lane 2, hexapodna; lane 3, pentapodna; lane 4, tetrapodna; lane 5, tripodna; lane 6, double-strand DNA; lane 7, single strand DNA. (C) CpG-ext(out) series: Lane 1, 20 bp DNA ladder; lane 2, single strand DNA; lane 3, double strand DNA; lane 4, tripodna; lane 5: tetrapodna; lane 6, pentapodna; lane 7, hexapodna. (D) CpG-ext(in) series: Lane 1, 20 bp DNA ladder; lane 2, single-strand DNA; lane 3, double-strand DNA; lane 4, tripodna; lane 5, tetrapodna; lane 6, pentapodna; lane 7, hexapodna.

number from 3 (tripodna) to 6 (hexapodna). When the polypodnas with an identical pod number were compared, little difference was observed in the migration distance. In contrast, the migration distances of the single-stranded CpG ODNs were different. This was due to the difference in the lengths of the CpG ODNs (ODN#1): the ODNs of the CpG-ext(out) and CpG-ext(in) series, Ext(out) ODN#1 and Ext(in) ODN#1, were 54 bases long, whereas those of the CpG-std and CpG-core series, Std ODN#1 and Core ODN#1, were 36 bases long.

Second, the Tm was measured to estimate the thermal stability of the polypodnas (Table 7). The Tm values were dependent on the pod number; the higher the pod number, the lower the Tm value. When the polypodnas with an identical pod number were compared, little difference was observed in Tm. An increase in the number of pods made each pod closer to the others within the polypodna structure, and the pods can cause steric repulsion among them. This may explain why the Tm values

Table 7. Melting temperatures (Tm) of polypodna preparations.

CpG-std	Tm (°C)	CpG-core	Tm (°C)	CpG-ext(out)	Tm (°C)	CpG-ext(in)	Tm (°C)
Hexapodna	57.4	Hexapodna	58.2	Hexapodna	57.7	Hexapodna	57.9
Pentapodna	58.4	Pentapodna	59.3	Pentapodna	58.8	Pentapodna	58.6
Tetrapodna	60.7	Tetrapodna	61.9	Tetrapodna	61.3	Tetrapodna	60.8
Tripodna	63.4	Tripodna	64.5	Tripodna	64.0	Tripodna	63.3
ds	73.5	ds	75.8	ds	74.9	ds	73.8

Tm was calculated from the thermal melting curves of polypodna preparations measured in 150 mM sodium chloride buffer, by using the derivative method.

tended to decrease as the pod number increased. Similar results were also found in our previous studies [30, 49, 84].

3.3.3 Cellular uptake and TNF-α release after addition of four series of polypodna to RAW264.7 cells

The release of TNF-α from RAW264.7 cells after the addition of four series of polypodnas is shown in Figure 17. The release of TNF-α followed an increasing trend as the pod number increased,

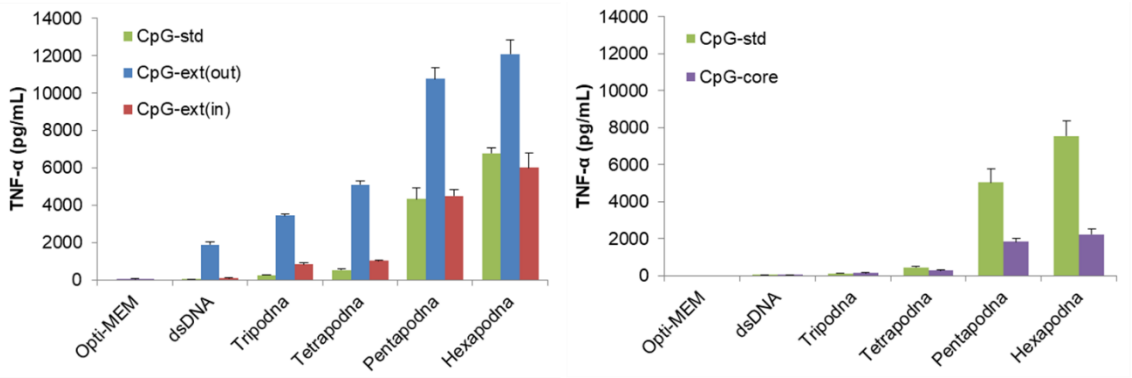

Figure 17. TNF- release from RAW264.7 cells following incubation with prepared DNA. Each sample in Opti-MEM was added to cells at a final concentration of 0.1 μM, and the concentration of TNF-α in the culture medium was measured at 8 h. (A) CpG-std, CpG-ext(out), and CpG-ext(in) series; (B) CpG-std and CpG-core series. The results are expressed as the mean ± SD of four measurements.

which was consistent with our previous findings [30, 31]. When the polypodnas with an identical pod number were compared, the CpG-ext(out) series exhibited the highest level of TNF-α release. The amounts of TNF-α were comparable between the CpG-ext(in) and CpG-std series. The CpG-core series exhibited the lowest level of TNF-α release. The uptake of Alexa Fluor 488-labeled polypodnas after addition to RAW264.7 cells is shown in Figure 18. Cellular uptake followed an increasing trend as the pod number increased. When the polypodnas with an identical pod number were compared, no significant difference was observed in cellular uptake. Collectively, these results suggested that the

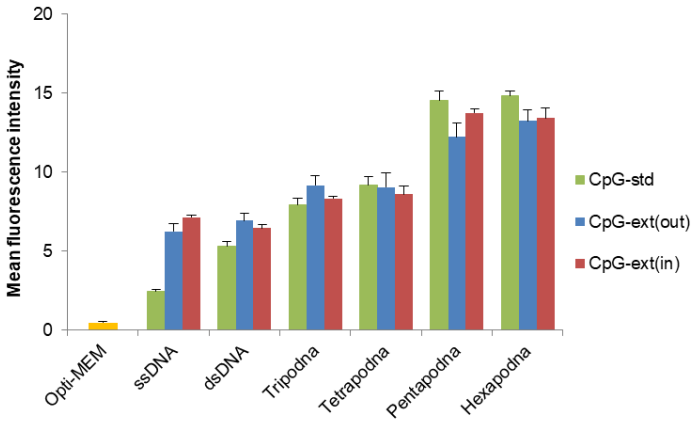

Figure 18. Uptake of polypodna preparations, ssDNA, and dsDNA by RAW264.7 cells. Each Alexa Fluor 488-labeled DNA sample was added to cells at a final concentration of 0.1 μM in Opti-MEM, and then the cells were incubated for 2 h at 37°C. The samples associated with cells were quantified by using flow cytometry, and the MFI was calculated to compare the cellular uptake of each preparation. CpG-std Hex01, CpG-ext(out) Hex01, and CpG-ext(in) Hex01 sequences were used as ssDNA. Te results are expressed as the mean ± SD of four measurements.

immunostimulatory activity of polypodnas was dependent on their structure and/or sequence, whereas their cellular uptake was not dependent on either parameter.

To achieve a more detailed comparison of the difference between CpG-ext(out) and CpG-ext(in), the TNF-α release and cellular uptake of CpG-ext(out) tetrapodna and CpG-ext(in) tetrapodna were examined over time. The time course of cellular uptake was comparable for both (Figure 19A), whereas CpG-ext(out) tetrapodna induced higher TNF-α release than CpG-ext(in) tetrapodna (Figure

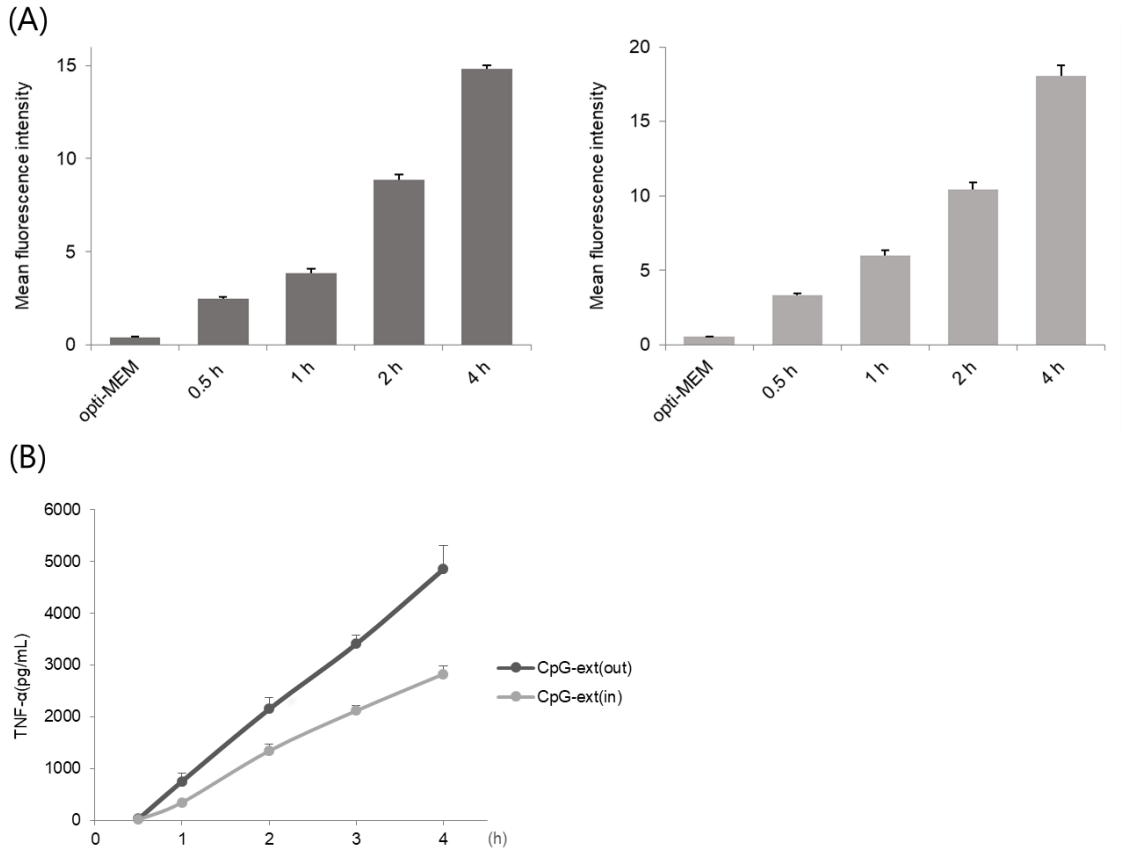

Figure 19. The relationship between cytokine release and cellular uptake in CpG-ext(out) and CpG-ext(in) tetrapodna. (A) The uptake of CpG-ext(out) (left) and CpG-ext(in) (right) tetrapodna. Alexa Fluor 488-labeled DNA samples were added to cells at a final concentration of 0.1 μM in Opti-MEM, and the cells were then incubated for 0.5, 1, 2, and 4 h at 37°C. The uptake of samples into cells was quantified using flow cytometry, and the MFI was calculated to compare the cellular uptake of each preparation. (B) TNF-α release from RAW264.7 cells by CpG-ext(out) and CpG-ext(in) tetrapodna. Each sample, diluted in Opti-MEM, was added to cells at a final concentration of 0.1 μM, and the concentration of TNF-α in the culture medium was measured at 0.5, 1, 2, and 4 h. The results are expressed as the mean ± SD of four measurements.

19B).

Many reports have emphasized that the CpG motif in single-stranded DNA is efficiently recognized by TLR9, which leads to cascade reactions [57, 58, 83]. The results of this study also showed that this rule could be applied to CpG motifs in three-dimensional structures such as polypodna. Among the four series of polypodna, the CpG-ext(out) series showed the highest TNF-α induction activity (Figure 17). The CpG motif in the CpG-ext(out) series is in the single-stranded part that is extended from the double-stranded part of the polypodna. Therefore, the motif can be recognized by TLR9 without dissociation into single-stranded ODNs. The CpG-ext(in) series has identical structural properties to the CpG-ext(out) series, including the extended single-stranded part, but the CpG motif of the CpG-ext(in) series is located in the double-stranded region. According to the literature, the CpG motif in double-stranded ODNs is hardly recognized by TLR9 [58]; thus the double-stranded ODNs need to dissociate into single-stranded ODNs to allow recognition of the CpG motif by TLR9. Therefore, the difference in the release of TNF-α between CpG-ext(out) and CpG-ext(in) (Figure 19) suggested the importance of the dissociation of the double-stranded parts for TLR9 recognition. The location of the CpG motif in double-stranded parts is also important for recognition. The CpG-core series resulted in the lowest TNF-α release, and the CpG motif in this series was the farthest from both ends of the ODN. Luo's group, by using fluorescence resonance energy transfer, reported that the Y-shaped DNA, which had structural properties identical to those of tripodna, dissociated from the three ends of the structure [54]. Therefore, ODNs consisting of polypodnas will dissociate from the 5′ and 3′ ends, and the CpG motif in the middle part of the polypodna becomes available for TLR9 recognition more slowly. This could provide an explanation for the rank order of the level of TNF-α release induced by the polypodna series (Figure 17).

3.3.4 Biological activity of single-strand CpG ODNs

The immunostimulatory activity of polypodnas containing CpG motifs is also affected by the potency of CpG ODNs to stimulate the immune responses. Therefore, the single-stranded CpG ODNs used for the preparation of polypodnas were added to RAW264.7 cells and TNF-α release from the cells was examined. Among the four kinds of single-stranded CpG ODNs, that is, Std ODN#1, Core ODN#1, Ext(in) ODN#1, and Ext(out) ODN#1, Ext(in) ODN#1 resulted in the highest level of TNF-α release, and Std ODN#1 resulted in the lowest level (Figure 20). This tendency was quite different from the results of the polypodnas. In conclusion, no apparent correlation in biological activity between single-stranded CpG ODNs and polypodnas was observed.

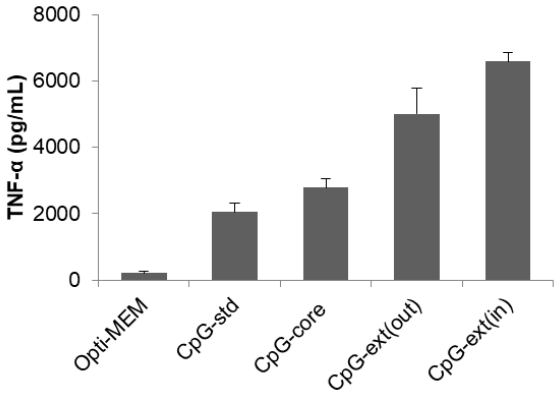

Figure 20. Cytokine release from RAW264.7 cells by single-strand DNA preparations. Each sample dissolved in Opti-MEM was added to cells at a final concentration of 0.1 μM, and the concentration of TNF-α in the culture medium were measured at 8 h. The results are expressed as the mean ± SD of four measurements.

Although many reports have demonstrated the relationship between the sequences of CpG ODN and their biological activities, most of these studies only focused on single- or double-stranded ODNs [57, 58, 83]. However, the findings of this study indicated that the rules obtained using single- or double-stranded CpG ODNs cannot be directly applied to CpG ODNs in polypodna. The results of the present study showed that the immunostimulatory activity of single-stranded CpG ODNs was mainly dependent on the length and base sequence because the differences in the cellular uptake of single-stranded CpG ODNs were small (Figure 18). The uptake of single-stranded CpG ODNs was significantly increased by their incorporation into polypodna, and the uptake efficiency was dependent on the structural properties, not on the base sequence. A study conducted in my laboratory demonstrated that cellular uptake increased as the pod number increased in the polypodna structure because of the increasing size [30]. This structure-dependent efficient uptake may reduce the importance of the base sequence in TLR9-mediated immune stimulation. These results have raised the concern that the immunostimulatory activity of single-strand CpG ODNs is not sufficient to estimate the activity after its incorporation into polypodna or other three-dimensional structures. The results also showed that the immunostimulatory activity of polypodna or other three-dimensional nanostructures can also be controlled by the length of the ODN and the position of the CpG motif.

Recently, Jelka *et al.* reported that although TLR9-mediated activation required single-stranded DNA longer than 20 nucleotides, CpG-containing ODNs as short as two nucleotides could augment the activation of TLR9 [85]. Another study also showed that DNA containing cytosine at the second position from the 5′ end bound to TLR9 in the presence of CpG DNA and cooperatively promoted the dimerization and activation of TLR9 [57]. Therefore, a strict design of the sequence is desired to optimize the TLR9-mediated immunostimulatory activity of CpG ODN in polypodna or other three-dimensional structures. Based on the results obtained in this study, the following rules can be proposed: First, the shape and size of a DNA nanostructure should be properly controlled because they determine the interaction and uptake by cells. Second, the base sequences of the CpG ODNs in

the nanostructure should be optimized. Moreover, safety evaluation is also an indispensable part of the development of nucleic acid medicine.

Conclusion

In Chapter 1, the AFM images indicate that the ODNs in the polypodnas, i.e., the tetra-, penta-, and hexapodnas, adopt the bend-type conformation when the structures are flattened under unconstrained conditions. The sequences around the junction have little effects on the bending angle or orientation of ODNs. These findings provide useful information concerning the coherent design of, and the structure–activity relationships for, a variety of DNA nanostructures.

In Chapter 2, I have demonstrated that the tetrapodna structure which contains the same palindrome sequences in the center can be formed in a tetrapod shape. Moreover, it also takes on a conformation similar to that of the symmetric tetrapodna, as determined by synchrotron X-ray scattering studies. The palindrome sequences did not reveal any negative influences in biological evaluations. These findings provide valuable information on creating more secure and reliable adjuvants and immunostimulatory agents.

In Chapter 3, I have designed four series of polypodna containing a CpG motif at varying positions, and demonstrated that the CpG motif in the single strand part of polypodna is more efficiently recognized by TLR9 than CpG in the double strand part after polypod-like structure-dependent efficient cellular uptake. Moreover, the tendency of immunoactivity of structured polypodna is hardly estimated by that of single strand CpG DNA. These findings provide valuable information for the sequence and structure optimization of polypodna and other nanosized DNA assemblies.

In conclusion, the results of this study are useful for elucidating the structure-activity relationship of DNA nanostructures, and they also provide useful information for designing safer and more efficient DNA nanostructures with immunostimulatory activity.

Acknowledgements

I have carried out these studies at Department of Biopharmaceutics and Drug Metabolism, Graduate School of Pharmaceutical Sciences, Kyoto University during Ph. D. course in 2017-2020. It would not be possible to do without the support and guidance that I received from many people.

First, I would like to express my sincere gratitude and thanks to Dr. Yoshinobu Takakura, Professor of Department of Biopharmaceutics and Drug Metabolism, Graduate School of Pharmaceutical Sciences, Kyoto University, for giving me wonderful opportunities and support with his patience, motivation, and immense knowledge. His guidance helped me in all the time of research and writing of this thesis.

I am extremely grateful to my research guides, Dr. Makiya Nishikawa, Professor of Laboratory of Biopharmaceutics, Faculty of Pharmaceutical Sciences, Tokyo University of Science, and Dr. Yuki Takahashi, Associate Professor of Department of Biopharmaceutics and Drug Metabolism, Graduate School of Pharmaceutical Sciences, Kyoto University, and Dr. Kosuke Kusamori, Assistant Professor of Laboratory of Biopharmaceutics, Faculty of Pharmaceutical Sciences, Tokyo University of Science. All of their encouragement, insightful comments, and hard questions are fully helpful and essential for my Ph. D. course.

I highly appreciate the supports received through the collaborative work provided from Dr. Hiroshi Sugiyama, Professor of Graduate School of Science, Kyoto University, Dr. Masayuki Endo, Associate Professor of Institute for Integrated Cell-Material Sciences, Kyoto University. They kindly supported on data collection in AFM imaging in Chapter 1. I also express my sincere appreciations to the collaborative works provided from Dr. Kazuo Sakurai, Professor of Department of Chemistry and Biochemistry, University of Kitakyushu. He kindly advised me on data analysis in SAXS profile in Chapter 2.

I would like to thank all of the students in the laboratory. They were always willing to help and give their best suggestions.

Finally, I would like to thank all of my family. They were always supporting and encouraging me with their best wishes.

References

1. Nishikawa, M., Tan, M., Liao, W., Kusamori, K. Nanostructured DNA for the delivery of therapeutic agents. *Adv Drug Deliv Rev.* 2019, *147*, 29-36.

2. Malik, S., Asmara, B., Moscato, Z., Mukker, J. K., Bahal, R. Advances in Nanoparticle-based Delivery of Next Generation Peptide Nucleic Acids. *Curr Pharm Des.* 2018, *24*, 5164-5174.

3. Xiang, D., Shigdar, S., Qiao, G., Wang, T., Kouzani, A. Z., Zhou, S., Kong, L., Li, Y., Pu, C., Duan, W. Nucleic Acid Aptamer-Guided Cancer Therapeutics and Diagnostics: the Next Generation of Cancer Medicine. *Theranostics.* 2018, *5*, 23-42.

4. Palmerston, M. L., Pan, J., Torchilin, V. P. Dendrimers as Nanocarriers for Nucleic Acid and Drug Delivery in Cancer Therapy. *Molecules.* 2017, *22*, 1401-1422.

5. Chen. J., Tang, Y., Liu, Y., Dou, Y. Nucleic Acid-Based Therapeutics for Pulmonary Diseases. *AAPS PharmSciTech.* 2018, *19*, 3670-3680.

6. Chen, C., Yang, Z., Tang, X. Chemical modifications of nucleic acid drugs and their delivery systems for gene-based therapy. *Med Res Rev.* 2018, *38*, 829-869.

7. Herrera, V. L., Colby, A. H., Ruiz-Opazo, N., Coleman, D. G., Grinstaff, M. W. Nucleic acid nanomedicines in Phase II/III clinical trials: translation of nucleic acid therapies for reprogramming cells. *Nanomedicine (Lond).* 2018, *13*, 2083-2098.

8. Hu, Q., Li, H., Wang, L., Gu, H., Fan, C. DNA nanotechnology-enabled drug delivery systems. *Chem. Rev.* 2019, *119*, 6459-6506.

9. Nadrian, C. Seeman., Hanadi, F. Sleiman. DNA nanotechnology. *Nat Rev Mater.* 2017, *3*, 1-23.

10. Lee, D. S., Qian, H., Tay, C. Y., Leong, D. T. Cellular processing and destinies of artificial DNA nanostructures. *Chem Soc Rev.* 2016, *45*, 4199-225.

11. Linko, V., Ora, A., Kostiainen, M. A. DNA nanostructures as smart drug-delivery vehicles and molecular devices. *Trends Biotechnol.* 2015, *33*, 586-594.

12. Um, S. H., Lee, J. B., Kwon, S. Y., Li, Y. G., Luo, D. Dendrimer-like DNA-based fluorescence nanobarcodes. *Nat. Protoc.* 2006, *1*, 995-1000.

13. Schmidt, M., Hagner, N., Marco, A., König-Merediz, S. A., Schroff, M., Wittig, B. Design and structural requirements of the potent and safe TLR-9 agonistic immunomodulator MGN1703. *Nucleic Acid Ther.* 2015, *25*, 130-40.

14. Kobiyama, K. Aoshi, T., Narita, H., Kuroda, E., Hayashi, M., Tetsutani, K., Koyama, S., Mochizuki, S., Sakurai, K., Katakai, Y., Yasutomi, Y., Saijo, S., Iwakura, Y., Akira, S., Coban, C., Ishii, K. J.

Nonagonistic Dectin-1 ligand transforms CpG into a multitask nanoparticulate TLR9 agonist. *Proc Natl Acad Sci U S A.* 2014, *111*, 3086-91.

15. Hanagata, N. CpG oligodeoxynucleotide nanomedicines for the prophylaxis or treatment of cancers, infectious diseases, and allergies. *Int J Nanomedicine.* 2017, *12*, 515-531.

16. Ke, Y., Ong, L. L., Shih, W. M., Yin, P. Three-dimensional structures self-assembled from DNA bricks. *Science.* 2012, *6111*, 1177-83.

17. Ke, Y., Ong, L. L., Sun, W., Song, J., Dong, M., Shih, W. M., Yin, P. DNA brick crystals with prescribed depths. *Nat Chem.* 2014, *11*, 994-1002.

18. Sajfutdinow, M., Jacobs, W. M., Reinhardt, A., Schneider, C., Smith, D. M. Direct observation and rational design of nucleation behavior in addressable self-assembly. *Proc Natl Acad Sci U S A.* 2018, 115, 5877-5886.

19. Dunn, K. E., Dannenberg, F., Ouldridge, T. E., Kwiatkowska, M., Turberfield, A. J., Bath, J. Guiding the folding pathway of DNA origami. *Nature.* 2015, *7567*, 82-6.

20. Ong, L. L., Hanikel, N., Yaghi, O. K., Grun, C., Strauss, M. T., Bron, P., Lai-Kee-Him, J., Schueder, F., Wang, B., Wang, P., Kishi, J. Y., Myhrvold, C., Zhu, A., Jungmann, R., Bellot, G., Ke, Y., Yin, P. Programmable self-assembly of three-dimensional nanostructures from 10,000 unique components. *Nature.* 2017, *7683*, 72-77.

21. Selnihhin, D., Sparvath, S. M., Preus, S., Birkedal, V., Andersen, E. S. Multifluorophore DNA origami beacon as a biosensing platform. *ACS Nano.* 2018, *12*, 5699-5708.

22. Rothemund, P. W. Folding DNA to create nanoscale shapes and patterns. *Nature.* 2006, *440*, 297-302.

23. Li. J., Pei. H., Zhu, B., Liang, L., Wei, M., He, Y., Chen, N., Li, D., Huang, Q., Fan, C. Self-Assembled Multivalent DNA Nanostructures for Noninvasive Intracellular Delivery of Immunostimulatory CpG Oligonucleotides. *ACS Nano.* 2011, *5*, 8783-9.

24. Ohtsuki, S., Matsuzaki, N., Mohri, K., Endo, M., Emura, T., Hidaka, K., Sugiyama, H., Takahashi, Y., Ishiyama, K., Kadowaki, N., Takakura, Y., Nishikawa, M. Optimal Arrangement of Four Short DNA Strands for Delivery of Immunostimulatory Nucleic Acids to Immune Cells. *Nucleic Acid Ther.* 2015, *25*, 245-53.

25. Lee, H., Lytton-Jean, A. K., Chen, Y., Love, K. T., Park, A. I., Karagiannis, E. D., Sehgal, A., Querbes, W., Zurenko, C. S., Jayaraman, M., Peng, C. G., Charisse, K., Borodovsky, A., Manoharan, M., Donahoe, J. S., Truelove, J., Nahrendorf, M., Langer, R., Anderson, D. G. Molecularly self-assembled nucleic acid nanoparticles for targeted in vivo siRNA delivery. *Nat Nanotechnol.* 2012, *7*, 389-93.

26. Mohri, K., Nishikawa, M., Takahashi, Y., Takakura, Y. DNA nanotechnology-based development of delivery systems for bioactive compounds. *Eur J Pharm Sci.* 2014, *58*, 26-33.

27. Yang, D., Hartman, M. R., Derrien, T. L., Hamada, S., An, D., Yancey, K. G., Cheng, R., Ma, M., Luo, D. DNA materials: bridging nanotechnology and biotechnology. *Acc Chem Res.* 2014, *47*, 1902-11.

28. Lee, J., Campolongo, M. J., Kahn, J. S., Roh, Y. H., Hartman, M. R., Luo, D. DNA-based nanostructures for molecular sensing. *Nanoscale.* 2010, *2*, 188-97.

29. Rattanakiat, S., Nishikawa, M., Funabashi, H., Luo, D., Takakura, Y. The assembly of a short linear natural cytosinephosphate-guanine DNA into dendritic structures and its effect on immunostimulatory activity. *Biomaterials.* 2009, *30*, 5701-5706.

30. Mohri, K., Nishikawa, M., Takahashi, N., Shiomi, T., Matsuoka, N., Ogawa, K., Endo, M., Hidaka, K., Sugiyama, H., Takahashi, Y., Takakura, Y. Design and development of nanosized
DNA assemblies in polypod-like structures as efficient vehicles for immunostimulatory CpG motifs to immune cells. *ACS Nano.* 2012, *6*, 5931-5940.

31. Sanada, Y., Shiomi, T., Okobira, T., Tan, M., Nishikawa, M., Akiba, I., Takakura, Y., Sakurai, K. Polypod-Shaped DNAs: Small-Angle X-ray Scattering and Immunostimulatory Activity. *Langmuir.* 2016, *32*, 3760-5.

32. Nishikawa, M., Ogawa, K., Umeki, Y., Mohri, K., Kawasaki, Y., Watanabe, H., Takahashi, N., Kusuki, E., Takahashi, R., Takahash,i Y., Takakura, Y. Injectable, self-gelling, biodegradable, and immunomodulatory DNA hydrogel for antigen delivery. *J Control Release.* 2014, *180*, 25-32.

33. Umeki, Y., Saito, M., Kusamori, K., Tsujimura, M., Nishimura, M., Takahashi, Y., Takakura, Y., Nishikawa, M. Combined encapsulation of a tumor antigen and immune cells using a self-assembling immunostimulatory DNA hydrogel to enhance antigen-specific tumor immunity. *J Control Release.* 2018, *288*, 189-198.

34. Yata, T., Takahashi, Y., Tan, M., Nakatsuji, H., Ohtsuki, S., Murakami, T., Imahori, H., Umeki, Y., Shiomi, T., Takakura, Y., Nishikawa, M. DNA nanotechnology-based composite-type gold nanoparticle-immunostimulatory DNA hydrogel for tumor photothermal immunotherapy. *Biomaterials.* 2017, *146*, 136-145.

35. Wemmer, D. E., Wand, A. J., Seeman, N. C., Kallenbach, N. R. NMR analysis of DNA junctions: Imino proton NMR studies of individual arms and intact junction. *Biochemistry.* 1985, *24*, 5745-5749.

36. Ortiz-Lombardía, M., González, A., Eritja, R., Aymamí, J., Azorín, F., Coll, M. Crystal structure of a DNA Holliday junction. *Nat. Struct. Biol.* 1999, *6*, 913-917.

37. Lilley, D. M. Structures of helical junctions in nucleic acids. *Q Rev. Biophys.* 2000, *33*, 109-159.

38. Li, Y. G., Tseng, Y. D., Kwon, S. Y., d'Espaux, L., Bunch, J. S., McEuen, P. L., Luo, D. Controlled assembly of dendrimer-like DNA. *Nat. Mater.* 2004, *3,* 38-42.

39. Mizuno, R., Haruta, H., Morii, T., Okada, T., Asakawa, T., Hayashi, K. Synthesis and AFM visualization of DNA nanostructures. *Thin Solid Films.* 2004, 459-465.

40. Lyubchenko, Y. L., Shlyakhtenko, L. S., Ando, T. Imaging of nucleic acids with atomic force microscopy. *Methods.* 2011, *54,* 274-283.

41. Nishikawa, M., Mizuno, Y., Mohri, K., Matsuoka, N., Rattanakiat, S., Takahashi, Y., Funabashi, H., Luo, D., Takakura, Y. Biodegradable CpG DNA hydrogels for sustained delivery of doxorubicin and immunostimulatory signals in tumor-bearing mice. *Biomaterials.* 2011, *32,* 488-494.

42. Endo, M., Katsuda, Y., Hidaka, K., Sugiyama, H. Regulation of DNA methylation using different tensions of double strands constructed in a defined DNA nanostructure. *J. Am. Chem. Soc.* 2010, *132,* 1592-1597.

43. Suzuki, Y., Endo, M., Katsuda, Y., Ou, K., Hidaka, K., Sugiyama, H. DNA origami based visualization system for studying site-specific recombination events. *J. Am. Chem. Soc.* 2014, *136,* 211-218.

44. Murchie, A. I. H., Clegg, R. M., von Krtzing, E., Duckett, D. R., Diekmann, S., Lilley, D. M. J. Fluorescence energy transfer shows that the four-way DNA junction is a righthanded cross of antiparallel molecules. *Nature.* 1989, *341,* 763-766.

45. Eichman, B. F., Vargason, J. M., Mooers, B. H. M., Ho, P. S. The Holliday junction in an inverted repeat DNA sequence: Sequence effects on the structure of four-way junctions. *Proc. Natl. Acad. Sci. USA.* 2000, *97,* 3971-3976.

46. Sha, R., Liu, F., Seeman, N. C. Atomic force microscopic measurement of the interdomain angle in symmetric Holliday junctions. *Biochemistry.* 2002, *41,* 5950-5955.

47. Peters 3rd, J. P., Maher, L. J. DNA curvature and flexibility in vitro and in vivo. *Q Rev. Biophys.* 2010, *43,* 23-63.

48. Vafabakhsh, R., Ha, T. Extreme bendability of DNA less than 100 base pairs long revealed by single-molecule cyclization. *Science.* 2012, *337,* 1097–1101.

49. Shiomi, T., Tan, M., Takahashi, N., Endo, M., Emura, T., Hidaka, K., Sugiyama, H., Takahashi, Y., Takakura, Y., Nishikawa, M. Atomic force microscopy analysis of orientation and bending of oligodeoxynucleotides in polypod-like structured DNA. *Nano Res.* 2015, *12,* 3764–3771.

50. Endo, M., Xing, X., Zhou, X., Emura, T., Hidaka, K., Tuesuwan, B., Sugiyama, H. Single-molecule manipulation of the duplex formation and dissociation at the G-quadruplex/i-motif site in the DNA nanostructure. *ACS Nano.* 2015, *10,* 9922-9.

51. Pabit, S. A., Katz, A. M., Tolokh, I. S., Drozdetski, A., Baker, N., Onufriev, A. V., Pollack, L. Understanding nucleic acid structural changes by comparing wide-angle x-ray scattering (WAXS) experiments to molecular dynamics simulations. *J Chem Phys.* 2016, *144*, 205102.

52. Shirazi, R. S., Ewert, K. K., Silva, B. F., Leal, C., Li, Y., Safinya, C. R. Structural evolution of environmentally responsive cationic liposome-DNA complexes with a reducible lipid linker. *Langmuir.* 2012, *28*, 10495-503.

53. Chatterjee, S., Lee, J. B., Valappil, N. V., Luo, D., Menon, V. M. Probing Y-shaped DNA structure with time-resolved FRET. *Nanoscale.* 2012, *5*, 1568-71.

54. Lee, J. B., Shai, A. S., Campolongo, M. J., Park, N., Luo, D. Three-dimensional structure and thermal stability studies of DNA nanostructures by energy transfer spectroscopy. *Chemphyschem.* 2010, *11*, 2081-4.

55. Pascal, T. A., Goddard, W. A., Maiti, P. K., Vaidehi, N. Role of specific cations and water entropy on the stability of branched DNA motif structures. *J Phys Chem B.* 2012, *116*, 12159-67.

56. Tavares, A. H. M. P., Pinho, A. J., Silva, R. M., Rodrigues, J. M. O. S., Bastos, C. A. C., Ferreira, P. J. S. G., Afreixo, V. DNA word analysis based on the distribution of the distances between symmetric words. *Sci Rep.* 2017, *7*, 728.

57. Ohto, U., Ishida, H., Shibata, T., Sato, R., Miyake, K., Shimizu, T. Toll-like receptor 9 contains two DNA binding sites that function cooperatively to promote receptor dimerization and activation. *Immunity.* 2018, *48*, 649-658.

58. Ohto, U., Shibata, T., Tanji, H., Ishida, H., Krayukhina, E., Uchiyama, S., Miyake, K., Shimizu, T. Structural basis of CpG and inhibitory DNA recognition by Toll-like receptor 9. *Nature.* 2015, *7549*, 702-5.

59. Sanada, Y., Sakamoto, S., Shiomi, T., Okobira, T., Mylonas, E., Ohta, N., Yagi, N., Nishikawa, M., Akiba, I., Takakura, Y., Sakurai, K. X-ray scattering from immunostimulatory tetrapod-shaped DNA in aqueous solution to explore its biological activity−conformation relationship. *J Phys Chem B.* 2014, *118*, 10373-9.

60. Im, K., Jeong, D., Hur, J., Kim, S. J., Hwang, S., Jin, K. S., Park, N., Kim, K. Robust analysis of synthetic label-free DNA junctions in solution by X-ray scattering and molecular simulation. *Sci Rep.* 2013, *3*, 3226.

61. Lindow, M., Vornlocher, H. P., Riley, D., Kornbrust, D. J., Burchard, J., Whiteley, L. O., Kamens, J., Thompson, J. D., Nochur, S., Younis, H., Bartz, S., Parry, J., Ferrari, N., Henry, S. P., Levin, A. A. Assessing unintended hybridization-induced biological effects of oligonucleotides. *Nat Biotechnol.* 2012, *30*, 920-3.

62. Naito, Y., Ui-Tei, K. Designing functional siRNA with reduced off-target effects. *Methods. Mol Biol.* 2013, *942*, 57-68.

63. Inagaki, H., Ohye, T., Kogo, H., Tsutsumi, M., Kato, T., Tong, M., Emanuel, B. S., Kurahashi, H. Two sequential cleavage reactions on cruciform DNA structures cause palindrome-mediated chromosomal translocations. *Nat Commun.* 2013, *4,* 1592.

64. Inagaki, H., Kato, T., Tsutsumi, M., Ouchi, Y., Ohye, T., Kurahashi, H. Palindrome-Mediated Translocations in Humans: A new mechanistic model for gross chromosomal rearrangements. *Front Genet.* 2016, *7*, 125.

65. Matsuoka, N., Nishikawa, M., Mohri, K., Rattanakiat, S., Takakura, Y. Structural and immunostimulatory properties of Y-shaped DNA consisting of phosphodiester and phosphorothioate oligodeoxynucleotides. *J Control Release*. 2010, *148,* 311-6.

66. Justin, P. Peters, L. James Maher, III. DNA curvature and flexibility in vitro and in vivo. *Q Rev. Biophys.* 2010, *43,* 23–63.

67. Bruetzel, L. K., Walker, P. U., Gerling, T., Dietz, H., Lipfert, J. Time-resolved small-angle X-ray scattering reveals millisecond transitions of a DNA origami switch. *Nano Lett.* 2018, *18,* 2672-2676.

68. Centlivre, M., Legrand, N., Klamer, S., Liu, Y. P., Jasmijn, von Eije. K., Bohne, M., Rijnstra, E. S., Weijer, K., Blom, B., Voermans, C., Spits, H., Berkhout, B. Preclinical in vivo evaluation of the safety of a multi-shRNA-based gene therapy against HIV-1. *Mol Ther Nucleic Acids.* 2013, *2,* e120.

69. Boudreau, R. L., Spengler, R. M., Davidson, B. L. Rational design of therapeutic siRNAs: minimizing off-targeting potential to improve the safety of RNAi therapy for Huntington's disease. *Mol Ther.* 2011, *19,* 2169-77.

70. Burdick, A. D., Sciabola, S., Mantena, S. R., Hollingshead, B. D., Stanton, R., Warneke, J. A., Zeng, M., Martsen, E., Medvedev, A., Makarov, S. S., Reed, L. A., Davis, J. W., Whiteley, L. O. Sequence motifs associated with hepatotoxicity of locked nucleic acid--modified antisense oligonucleotides. *Nucleic Acids Res.* 2014, *42,* 4882-91.

71. Monteys, A. M., Spengler, R. M., Dufour, B. D., Wilson, M. S., Oakley, C. K., Sowada, M. J., McBride, J. L., Davidson, B. L. Single nucleotide seed modification restores in vivo tolerability of a toxic artificial miRNA sequence in the mouse brain. *Nucleic Acids Res.* 2014, *42,* 13315-27.

72. Ko, S., Liu, H., Chen, Y., Mao, C. DNA nanotubes as combinatorial vehicles for cellular delivery. *Biomacromolecules.* 2008, *11,* 3039-43.

73. Weiner, G. J., Liu, H. M., Wooldridge, J. E., Dahle, C. E., Krieg, A. M. Immunostimulatory oligodeoxynucleotides containing the CpG motif are effective as immune adjuvants in tumor antigen immunization. *Proc Natl Acad Sci U S A.* 1997, *94,* 10833-7.

74. Krieg, A. M. CpG motifs in bacterial DNA and their immune effects. *Annu Rev Immunol.* 2002, *20,* 709-60.

75. Takeda, K., Akira, S. Toll-like receptors. *Curr Protoc Immunol.* 2015, *1,* 109-14.

76. Vollmer, J., Krieg, A. M. Immunotherapeutic applications of CpG oligodeoxynucleotide TLR9 agonists. *Adv Drug Deliv Rev.* 2009, *61,* 195-204.

77. Krug, A., Rothenfusser, S., Hornung, V., Jahrsdörfer, B., Blackwell, S., Ballas, Z. K., Endres, S., Krieg, A. M., Hartmann, G. Identification of CpG oligonucleotide sequences with high induction of IFN-alpha/beta in plasmacytoid dendritic cells. *Eur J Immunol.* 2001, *31,* 2154-63.

78. Krieg, A. M., Yi, A. K., Matson, S., Waldschmidt, T. J., Bishop, G. A., Teasdale, R., Koretzky, G. A., Klinman, D. M. CpG motifs in bacterial DNA trigger direct B-cell activation. *Nature.* 1995, *374,* 546-9.

79. Hartmann, G., Weeratna, R. D., Ballas, Z. K., Payette, P., Blackwell, S., Suparto, I., Rasmussen, W. L., Waldschmidt, M., Sajuthi, D., Purcell, R. H., Davis, H. L., Krieg, A. M. Delineation of a CpG phosphorothioate oligodeoxynucleotide for activating primate immune responses in vitro and in vivo. *J Immunol.* 2000, *164,* 1617-24.

80. Pohar, J., Yamamoto, C., Fukui, R., Cajnko, M. M., Miyake, K., Jerala, R., Benčina, M. Selectivity of Human TLR9 for Double CpG Motifs and Implications for the Recognition of Genomic DNA. *J Immunol.* 2017, *198,* 2093-2104.

81. Pohar, J., Kužnik, Krajnik. A., Jerala, R., Benčina, M. Minimal sequence requirements for oligodeoxyribonucleotides activating human TLR9. *J Immunol.* 2015, *194,* 3901-8.

82. Pohar, J., Lainšček, D., Fukui, R., Yamamoto, C., Miyake, K., Jerala, R., Benčina, M. Species-Specific Minimal Sequence Motif for Oligodeoxyribonucleotides Activating Mouse TLR9. *J Immunol.* 2015, *195,* 4396-405.

83. Majer, O., Liu, B., Barton, G. M. Nucleic acid-sensing TLRs: trafficking and regulation. *Curr Opin Immunol.* 2017, *44,* 26-33.

84. Tan, M., Takahashi, N., Fujii, S., Sakurai, K., Kusamori, K., Takahashi, Y., Takakura, Y., Nishikawa, M. Analysis of Tertiary Structural Features of Branched DNA Nanostructures with Partially Common Sequences Using Small-Angle X-ray Scattering. ACS Appl. Bio Mater. 2020, 3, 308-314.

85. Pohar, J., Lainšček, D., Ivičak-Kocjan, K., Cajnko, M. M., Jerala, R., Benčina, M. Short single-stranded DNA degradation products augment the activation of Toll-like receptor 9. *Nat Commun.* 2017, *8,* 15363-15376.

86. Jackson, S., Lentino, J., Kopp, J., Murray, L., Ellison, W., Rhee, M., Shockey, G., Akella, L., Erby, K., Heyward, W. L., Janssen, R. S., HBV-23 Study Group. Immunogenicity of a two-dose

investigational hepatitis B vaccine, HBsAg-1018, using a toll-like receptor 9 agonist adjuvant compared with a licensed hepatitis B vaccine in adults. *Vaccine*. 2018, *36*, 668-674.
87. Monteith, D. K., Horner, M. J., Gillett, N. A., Butler, M., Geary, R., Burckin, T., Ushiro-Watanabe, T., Levin, A. A. Evaluation of the renal effects of an antisense phosphorothioate oligodeoxynucleotide in monkeys. *Toxicol Pathol.* 1999, *27*, 307-317.